

Co-development of Jurassic I-type and A-type granites in southern Hunan, South China: Dual control by plate subduction and intraplate mantle upwelling



Hua Kong^a, Huan Li^{a,*}, Qian-Hong Wu^a, Xiao-Shuang Xi^a, Jeffrey M. Dick^a, Jillian Aira S. Gabo-Ratio^b

^a Key Laboratory of Metallogenetic Prediction of Nonferrous Metals and Geological Environment Monitoring, Ministry of Education, School of Geosciences and Info-Physics, Central South University, Changsha 410083, China

^b National Institute of Geological Sciences, University of the Philippines, Diliman, Quezon City 1101, Philippines

ARTICLE INFO

Handling Editor: Orhan Karsli

Keywords:

I-type granites
A-type granites
Zircon Hf isotope
Plate subduction
Mantle upwelling
South Hunan

ABSTRACT

Two types of spatially and temporally associated Jurassic granitic rocks, I-type and A-type, occur as pluton pairs in several locations in southern Hunan Province, South China. This paper aims to investigate the genetic relationships and tectonic mechanisms of the co-development of distinct granitic rocks through petrological, geochemical and geochronological studies. Zircon LA-ICPMS dating results yielded concordant U-Pb ages ranging from 180 to 148 Ma for the Baoshan and Tongshanling I-type granodiorites, and from 180 to 158 Ma for the counterpart Huangshaping and Tuling A-type granites. Petrologically, the I-type granodiorites consist of mafic minerals such as hornblende whereas the A-type granites are dominated by felsic minerals (e.g., quartz, K-feldspar and plagioclase). Major and trace element analyses indicate that the I-type granodiorites have relatively low SiO₂ (64.5–71.0%) and relatively high TiO₂ (0.28–0.51%), Al₂O₃ (13.8–15.5%), total FeO (2.3–4.7%), MgO (1.3–2.6%) and P₂O₅ (0.10–0.23%) contents, and the A-type granites are characterized by high concentrations of Rb (212–1499 ppm), Th (18.3–52.6 ppm), U (11.8–33.6 ppm), Ga (20.0–36.6 ppm), Y (27.1–134.0 ppm) and HREE (20.3–70.0 ppm), with pronounced negative Eu anomalies (Eu/Eu^{*} = 0.01–0.15). Moreover, the I-type granodiorites are classified as collision-related granites emplaced under a compressional environment, whereas the A-type granites are within-plate granites generated in an extensional setting. Zircon Hf isotopic compositions vary substantially for these granitic rocks. The I-type granodiorites are characterized by relatively young Hf model ages ($T_{DM1} = 1065$ –1302 Ma, $T_{DM}^C = 1589$ –2061 Ma) and moderately negative $\epsilon\text{Hf}(t)$ values (-5.9 to -11.5), whereas the A-type granites have very old model ages ($T_{DM1} = 1454$ –2215 Ma, $T_{DM}^C = 2211$ –2974 Ma) and pronounced negative $\epsilon\text{Hf}(t)$ values (-15.8 to -28.3). These petrochemical and isotopic characteristics indicate that the I-type granodiorites may have been derived from a deep source involving mantle-derived juvenile (basaltic) and crustal (pelitic) components, whereas the A-type granites may have been sourced from melting of meta-greywacke in the crust. This study proposes that the pressure and temperature differences in the source regions caused by combined effects of intra-plate mantle upwelling and plate subduction are the major controlling factors of the co-development of the two different types of magmas. Crustal anatexis related to lithospheric delamination and upwelling of hot asthenosphere under a high pressure and temperature environment led to the formation of the I-type magmas. On the other hand, the A-type magmas were formed from melting of the shallower part of the crust, where extensional stress was dominant and mantle-crust interaction was relatively weak. Rifts and faults caused by mantle upwelling developed from surface to depth and successively became channels for the ascending I- and A-type magmas, resulting in the emplacement of magmas in adjacent areas from sources at different depths.

* Corresponding author at: Key Laboratory of Metallogenetic Prediction of Nonferrous Metals and Geological Environment Monitoring, Ministry of Education, School of Geosciences and Info-Physics, Central South University, Changsha 410083, China.

E-mail address: lihuan@csu.edu.cn (H. Li).

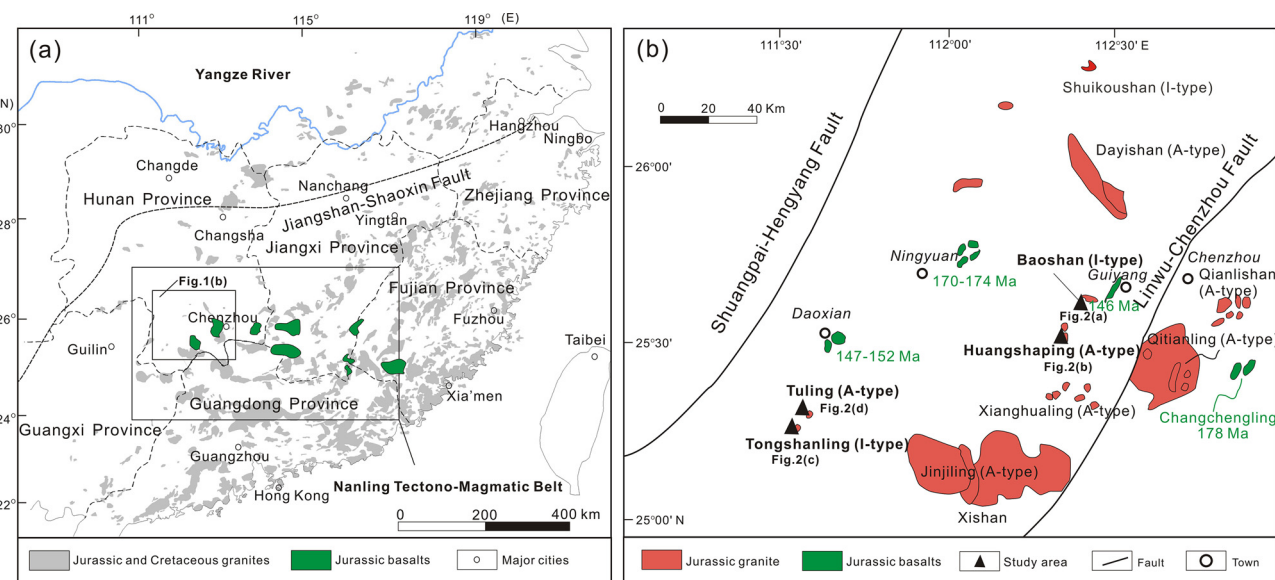


Fig. 1. (a) Distribution of the Jurassic–Cretaceous granitic plutons and Jurassic basaltic rocks in South China (after Li et al., 2009; Liu et al., 2012). (b) Distribution of the Jurassic granites and basalts in the South Hunan region (after Jiang et al., 2009; Li et al., 2014a).

1. Introduction

South China is characterized by widely distributed Jurassic and Cretaceous granites and abundant mineral resources (Fig. 1a). Compared with those in other regions, the Jurassic granites in South China show complex genetic types and distinct formation processes, and have a close affinity with metallogenesis (Zhou and Li, 2000; Zhou et al., 2006; Xu, 2008; Huang et al., 2017; Li et al., 2017a, 2018a; Jiang et al., 2018a, 2018b). Studies in the past century have gradually revealed the temporal and spatial distribution of the granites, and their diversity has been attributed to different source rocks and geodynamic settings and varied degrees of crust-mantle interactions (Hsu et al., 1990; Chen et al., 2002; Cao et al., 2018a, 2018b). However, due to their high diversity and complexity, the specific relationships between granite types, source regions and tectonic settings of these Jurassic granites have not been well clarified.

The Jurassic granites in South China, which mainly consist of biotite granite, two-mica granite and muscovite granite, have already been differentiated into S- and I-type by previous studies (Chen and Jahn, 1998; Zeng et al., 2001; Hua et al., 2003; Yang et al., 2016). The S-type granites were interpreted to be derived from the regional Paleoproterozoic meta-sedimentary rocks (Hua et al., 2007), whereas the I-type granites originated from infracrustal igneous rocks and were generated by mixing of mantle- and crust-derived materials (Wang and Shen, 2003). More recently, increasing numbers of Jurassic granites in South China, which were previously considered to be S- or I-type, have been reclassified as A-type granites (e.g., Li et al., 2007a, 2007b; Wang et al., 2015; Zhang et al., 2015; Li et al., 2018b, 2018c). These A-type granites are generally thought to have formed in an extensional setting (Zhou and Li, 2000; Li and Li, 2007), but their source regions and tectonic attributes are still a topic of debate (Chen et al., 2002; Zhu et al., 2011; Zhao et al., 2012; Chen et al., 2016). In addition, the relationship between these varied granite types as well as their combined implications for the Jurassic tectonic regime in South China requires further investigation.

The tectonic genesis of large-scale magmatism in South China has been discussed for many years with two opposing views: 1) Andean-type active continental margin setting generated by subduction of the paleo-Pacific plate, or 2) intra-plate lithospheric thinning and intracontinental reworking (Wang et al., 2013). The former is represented by models of active continental margin or back-arc extension (Zhou and

Li, 2000), break-up of a subducted flat slab (Li et al., 2007b) and oblique subduction of the Pacific plate (Wang et al., 2011). The latter is illustrated by models of a super mantle plume that generated a G (granite)-type large igneous province (Zhang et al., 2009) and triple junction rifting system (Quan et al., 2013b). Though these models offer important insights into the evolution of tectonic processes in Jurassic South China, they are still under debate and have not been universally agreed upon. These single tectonic models are also limited in scope and therefore cannot account for the diversity of granites in South China. Moreover, it has not been established whether the combined effects of plate subduction and intraplate mantle upwelling influenced the genesis of diversified granitic magmas.

The central Nanling region (especially southern Hunan Province) has various types of Mesozoic granitoids and ore deposits and is considered to be the most important geological component of South China. These granitoids are classified as I- and A-type granites, corresponding to Cu-Au and W-Sn-Mo-Bi-Pb-Zn polymetallic mineralization, respectively (Mao et al., 2013; Li et al., 2014b; Yang et al., 2016; Zhao et al., 2016). The I-type granitoids in this region are represented by the Baoshan, Tongshanling and Shuikoushan granitic plutons, whereas the A-type granites mainly include the Huangshaping, Qianlishan, Qitianling, Dayishan, Jinjiling, Xianghualing, and Tuling plutons (Fig. 1b). The genesis of these spatially and temporally associated I- and A-type granites in South Hunan is still controversial and a conclusive interpretation of their genetic relationship has not yet been proposed. Previous research ascribed the co-development of the I- and A-type granites to differences in either the lithospheric compositions (Zhang et al., 2000) or intruding depths of the granite bodies (Bai et al., 2007). However, detailed investigations of the differences in source composition and geodynamic setting of the magma source region were not carried out. In addition, the relationship between magma genesis and the tectonic setting in South Hunan and adjacent areas is still under debate (e.g., Li et al., 2007a, 2007b; Zhang et al., 2009; Quan et al., 2013b). In order to better understand the origin of the contemporaneous I- and A-type magmatism in South Hunan, a detailed study was carried out on the two pairs of co-developed I- and A-type intrusions in southern Hunan Province, South China. In this contribution, geochronological, petrological, and geochemical data for the Baoshan (I-type), Huangshaping (A-type), Tongshanling (I-type) and Tuling (A-type) granitic intrusions are reported to constrain their petrogenesis, discuss the tectonic implications, and gain new insights on

the variable attributes of the magma source region beneath the South China Block during the Jurassic.

2. Regional geology

South China experienced multiple orogenic, magmatic and metagenic processes since the Neoproterozoic era (Charvet, 2013; Wang et al., 2013). It is composed of the Yangtze Block to the northwest and the Cathaysia Block to the southeast. These two blocks finally amalgamated along a Neoproterozoic collision belt (Jiangnan orogen) at 860 to 800 Ma (Zhao and Cawood, 2012; Yao et al., 2016; Zhao, 2016; Li et al., 2016a). The Jiangshan-Shaoxing fault (suture) is the southern boundary of this orogen, with an undetermined westward extension of the fault trace (Hu et al., 2012; Fig. 1a). The early Paleozoic orogen in South China has been proposed to represent the first important crustal reworking since the Neoproterozoic (Li et al., 2010). Lower- to middle-crustal anatexis, asthenospheric mantle upwelling and activation of the pre-existing suture zones resulted in early Paleozoic magmatism (Xu and Xu, 2015; Zhang et al., 2016a). Afterwards the region entered a new stage of Mesozoic intraplate continental dynamic evolution but simultaneously was affected by the subduction of the Pacific plate (Chen et al., 2002; Yu et al., 2010).

Continental-wide extension was the major tectonic process in South China during the Late Mesozoic (Jurassic and Cretaceous), characterized by faulting, half-grabens and magmatic intrusions in a vast area ($\sim 110,000 \text{ km}^2$) (Hsieh et al., 2008; Wei et al., 2016). Extensional basins (half grabens) developed since the Early Jurassic in the eastern part of South China (i.e., in the Hunan, Jiangxi and Guangdong provinces (Shu et al., 2009)) and experienced exhumation during the Middle Jurassic (Pang et al., 2014); these were coupled with bimodal volcanic sequences that erupted in the Nanling range (Zhou et al., 2006). The early-middle Jurassic (dominantly 195–170 Ma) basaltic and rhyolitic rocks outcrop along the Nanling Range from southern Hunan through southern Jiangxi and finally to southeastern Fujian, and are spatially associated with subsequently emplaced calc-alkaline granite, A-type granite and syenite (Fig. 1a, He et al., 2010; Wang et al., 2013). The middle Jurassic basaltic rocks in this zone exhibit a geochemical affinity to OIB-like composition (Zhou et al., 2006; Cen et al., 2016), and some late Jurassic mafic rocks in this zone also show a significant affinity to an enriched subcontinental lithospheric mantle source (Wang et al., 2008). The Late Mesozoic I-, S- and A-type granitoid rocks generally display younger crystallization ages toward the coastal regions, occurring as an array which is oblique to the coastal provinces of southeast China (Zhou and Li, 2000; Wang et al., 2013). Coinciding with the timing of a change from basin subsidence to basin shallowing, the Jurassic granitoids were formed at 180–152 Ma and are mostly located in the inland provinces. The Cretaceous magmatic rocks were formed at two intervals of ca. 130–120 Ma and 107–87 Ma, and are mainly distributed in the coastal provinces (Deng et al., 2014; Li et al., 2015). The Cretaceous rocks are composed of A-type granitoids, adakitic rocks, and volcanics that mainly consist of tuff, basalt and rhyolite, implying an extensional setting (Li et al., 2014c, 2016b). Collectively, the Jurassic intraplate granite-syenite-gabbro association is considered to be a response to far-field stress from the paleo-Pacific plate subduction (Wang et al., 2013). These rock types are interpreted as the products of the interaction between the lithospheric crust and the asthenospheric mantle in a rift-like setting (Zhou et al., 2006; Li et al., 2007a, 2007b; He et al., 2010).

The southern Hunan Province, which makes up the central Nanling region, is characterized by complex geologic conditions and rich mineral resources. It experienced complex tectonic movement in different stages and to varying degrees, accompanied by magmatic activities (Mao et al., 2013). The Caledonian movement resulted in the metamorphism of the Cambrian–Sinian sedimentary rocks and the folding and uplift of the basement in South Hunan. Subsequently, Devonian–Permian carbonate rocks were heavily folded and their

successions were generally deformed during the Late Permian–Triassic. Finally, Jurassic–Cretaceous tectonic activity led to the formation of NNE-directed rift-related basins and deep faults. Aside from the sedimentary and metamorphic units, magmatic rocks are also widely distributed in this area. Among them, Jurassic magmatic activity played the most important role in the formation of granitic composites and mineral resources. The Jurassic granites (180–150 Ma) are characterized by multiple stages of intrusions that are associated with abundant polymetallic ore deposits (Peng et al., 2006; Yuan et al., 2008; Li et al., 2017a). Middle to late Jurassic mafic magmatism can be also found in southern Hunan (Fig. 1b). This includes the Changchengling basalt–basaltic andesite association (178 Ma; Zhao et al., 1998), Ningyuan alkali basalt–trachybasalt–shoshonite association (174–170 Ma, Li et al., 2004), Daoxian basaltic lavas (152–147 Ma, Li et al., 2004) and Guiyang lamprophyre dykes which have mineral components of trachybasalt and shoshonite (146 Ma, Wang et al., 2003). The intensive Jurassic magmatism in this region either occurred in an intra-plate rift-related environment or was affected by the subduction of the paleo-Pacific plate (Jiang et al., 2009; Wang et al., 2011; Li et al., 2014a, 2014b; Wu et al., 2016).

The Baoshan granitic intrusion is located in the northern part of central Nanling region (Fig. 2a; Quan et al., 2012a). It consists of two intrusive phases: porphyritic granodiorite and granodiorite porphyry. These two types of magmatic rocks occur as small dikes that intrude into Devonian and Carboniferous sedimentary rocks along faults. The porphyritic granodiorite is dark grey in colour and has a porphyritic-like texture with quartz, plagioclase, K-feldspar, hornblende and biotite as phenocrysts and the same mineral paragenesis as a fine-grained ($< 0.02 \text{ mm}$) groundmass (Fig. 3a, b). The granodiorite porphyry, which is also dark grey in colour, has a porphyritic texture with quartz, plagioclase, K-feldspar and biotite as its phenocrysts (Fig. 3c, d), and is a hypabyssal-type intrusive rock. The Huangshaping granitic body is located in the central portion of the Nanling region and is close to the Baoshan intrusion (Fig. 2b; Quan et al., 2012b; Li et al., 2017a). It is composed of three intrusive phases, outcropping quartz porphyry, unexposed granophyre, and granite porphyry. The concealed granophyre bodies are in fault contact with the quartz porphyry, and both of them are isolated from the granite porphyry bodies that are located in the southeast portion of the area. Phenocrysts of the quartz porphyry are mainly composed of quartz and minor feldspar and biotite. The groundmass of this porphyry also consists of quartz and feldspars, with a felsitic texture (Fig. 3e, f), showing a hypabyssal-type characteristic. The granophyre is characterized by a granophytic texture with K-feldspar, quartz and small amounts of plagioclase and biotite as phenocrysts. The groundmass of this porphyry has a micrographic texture (Fig. 3g, h). The granite porphyry has a typical porphyritic texture with quartz, K-feldspar and minor plagioclase and biotite phenocrysts. The groundmass is characterized by a fine-grained granitic texture (Fig. 3i, j). The Tongshanling granodiorite bodies are located in the western portion of the central Nanling region (Fig. 2c; Quan et al., 2013a). These bodies are randomly distributed, showing no clear spatial relations with each other. The granodiorite from the major intrusive body (intrusion I) is characterized by a porphyritic texture, with coarse-grained K-feldspar and plagioclase phenocrysts and fine-grained quartz, plagioclase, biotite and K-feldspar groundmass (Fig. 3k, l). The granodiorites from the secondary bodies (intrusions II and III) are porphyritic, light grey in colour and contain quartz veins, with medium-grained K-feldspar and plagioclase phenocrysts and groundmass of fine-grained quartz, plagioclase, hornblende, biotite and K-feldspar (Fig. 3m, n). The Tuling pluton is 15 km northeast of the Tongshanling pluton (Fig. 2d), and is mainly composed of granite porphyry. This hypabyssal-type intrusive rock has a porphyritic texture with K-feldspar, quartz and biotite phenocrysts and groundmass of fine-grained quartz, feldspar, plagioclase and biotite (Fig. 3o, p).

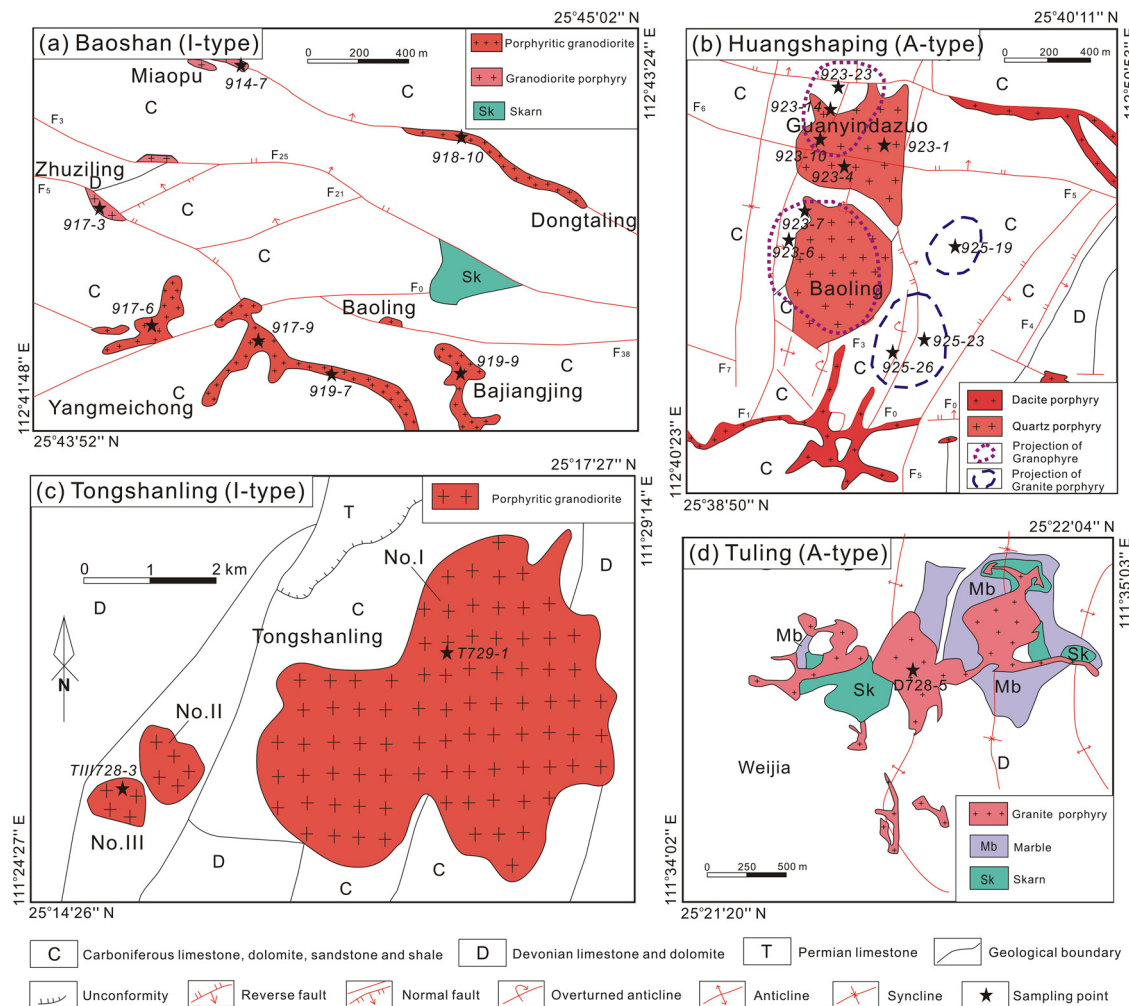


Fig. 2. Simplified geological maps of (a) Baoshan, (b) Huangshaping, (c) Tongshanling and (d) Tuling areas. (a) is after Quan et al. (2012a), (b) is after Li et al. (2014b), (c) is after Quan et al. (2013a, 2013b), and (d) is after Yang et al. (2012). The sampling locations in (a) and (b) are projected points of underground samples, and in (c) and (d) are surface samples in this study.

3. Sampling, analytical techniques and data processing

Different types of granitic rocks were collected from outcrops and in mining tunnels in southern Hunan. Sampling locations are shown in Fig. 2.

Whole rock major and trace element analyses were carried out at the Wuhan Comprehensive Rock and Mineral Analysis Center (Hubei Geological Research Laboratory, China). Major elements were analyzed using an X-ray fluorescence spectrometer (XRF) with a relative analytical precision < 1%. Fe²⁺ and Fe³⁺ were analyzed using a wet chemical method. Rare earth and other trace elements were analyzed using inductively coupled plasma mass spectrometry (ICP-MS). A standard sample was also used to monitor the reliability of analytical results, and the accuracy for most trace elements was better than 5%.

Zircon crystal separation was carried out using standard techniques. Crystals were picked by hand under a binocular microscope, and mounted in epoxy resin and polished down to expose the grain center. Cathodoluminescence (CL) images were taken for all zircons at Northwest University, China. In situ U-Pb isotopic analyses were carried out using laser ablation-inductively coupled plasma-mass spectrometry (LA-ICP-MS), also at Northwest University. An ArF-excimer 193 nm laser ablation system (GeoLas 200 M) and an Agilent 7500a ICP-MS instrument were used to acquire ion-signal intensities. The laser spot size was 32 μm, and the ablation depth was controlled at 20–40 μm. Helium was used as the carrier gas. For each analysis, a gas

blank was acquired for 20 s prior to the laser ablation of 30 s duration. Zircon 91,500 and GJ-1 were used as the calibration references for U-Pb dating, and were analyzed twice for every five samples. Every series of 10 analytical spots for samples was followed by one analysis of NIST SRM 610 standard to correct for the time-dependent drift of sensitivity and mass discrimination in the trace element analysis. Detailed analytical conditions and procedures for the LA-ICPMS zircon U-Pb dating are described in Yuan et al. (2004) and Diwu et al. (2012). Off-line selection and integration of background and analytical signals, time-drift correction, and quantitative calibration for zircon U-Pb dating were performed using the ICPMSDataCal software (version 8.3). Concordia diagrams and weighted mean calculations were made using Isoplot 4.5 (Ludwig, 2003).

High spatial resolution Hf isotopic analyses were carried out at Northwest University for dated zircon crystals with concordant ages using a Neptune MC-ICPMS with an ArF excimer laser ablation system. The ablation spots for the Hf isotope analyses were situated adjacent to the U-Pb age analysis positions on each grain. During analyses, a spot size of 44 μm, an ablation depth of 20–40 μm, a laser repetition rate of 10 Hz, and an energy density of 5.3 J/cm² were used. The ablation time was 120 s for each analysis. Zircon 91500, MON-1 and GJ-1 were used as the reference materials. For the detailed analytical procedures and isobaric interference corrections, refer to the descriptions in Wu et al. (2006) and Zhang et al. (2016b).

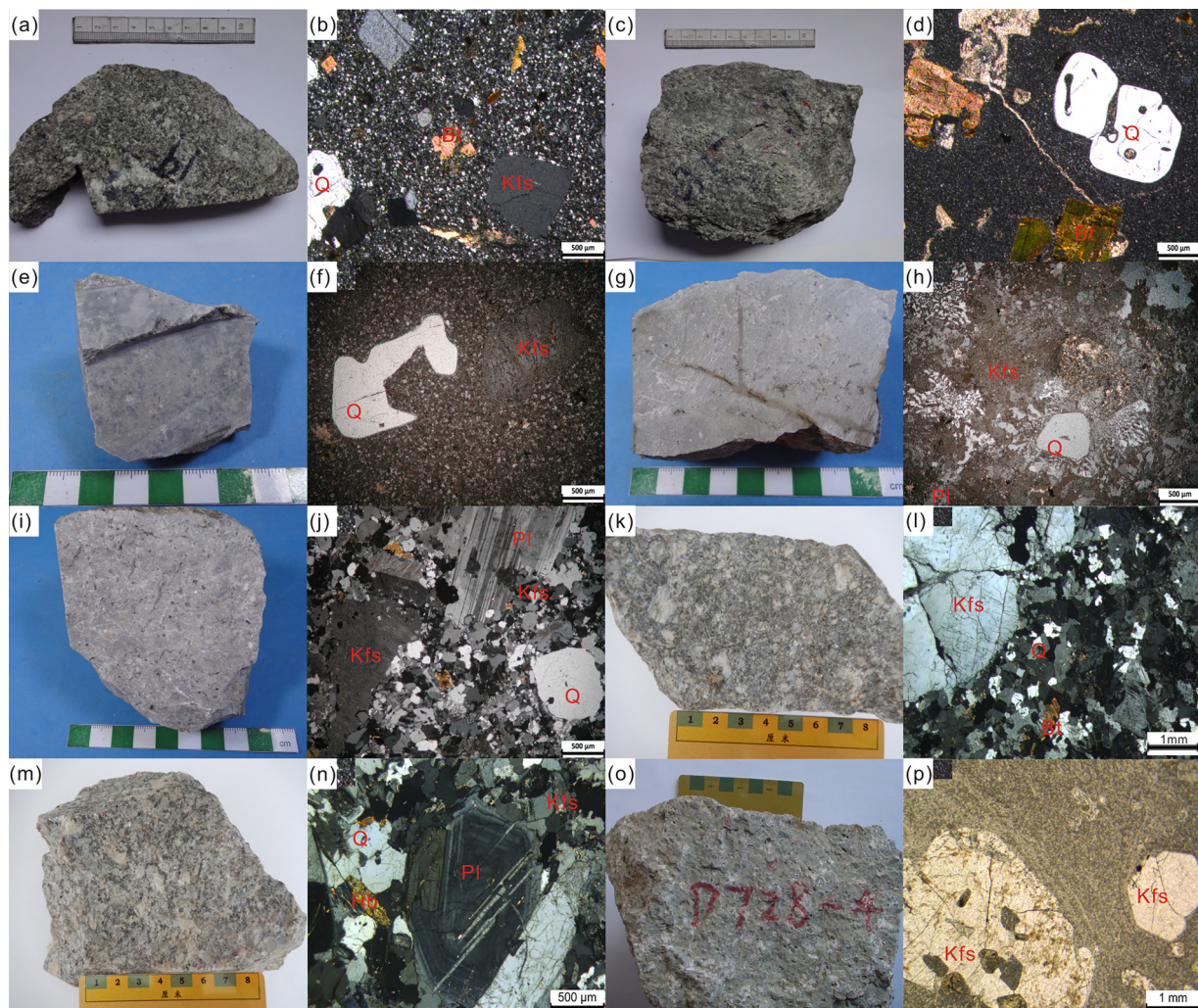


Fig. 3. Hand specimen images and photomicrographs of the granitic rocks from South Hunan. (a–b) porphyritic granodiorite in Baoshan (micro-crystalline porphyritic texture), (c–d) granodiorite porphyry in Baoshan, (e–f) quartz porphyry in Huangshaping, (g–h) granophyre in Huangshaping, (i–j) granite porphyry in Huangshaping, (k–l) porphyritic granodiorite from the major intrusive body (intrusion I) in Tongshanling, (m–n) porphyritic granodiorite from intrusion III in Tongshanling (medium-crystalline porphyritic texture), (o–p) granite porphyry in Tuling. More detailed interpretations can be found in the text. Q: Quartz, Bt: Biotite, Kfs: K-feldspar, Pl: Plagioclase, Hb: hornblende.

4. Results

4.1. Major and trace elements

Major and trace element concentrations of the granitic rock samples from the four areas are shown in Table 1. The loss on ignition (LOI) for most samples is less than 2 wt. %, indicating that alteration and weathering are negligible. These granitic rocks have a wide range of chemical compositions and can be divided into two groups based on their elemental variations. The Baoshan and Tongshanling granodiorites are characterized by low SiO_2 but high TiO_2 , Al_2O_3 , CaO , total FeO , MgO , MnO and P_2O_5 concentrations (Fig. 4a–f), with $\text{SiO}_2 = 64.5\text{--}71.0\%$, $\text{TiO}_2 = 0.28\text{--}0.60\%$, $\text{Al}_2\text{O}_3 = 13.7\text{--}15.5\%$, $\text{CaO} = 1.6\text{--}4.3\%$, $\text{FeO} = 1.4\text{--}3.7\%$, $\text{Fe}_2\text{O}_3 = 0.75\text{--}1.3\%$, $\text{MgO} = 1.3\text{--}2.6\%$, $\text{MnO} = 0.05\text{--}0.17\%$ and $\text{P}_2\text{O}_5 = 0.09\text{--}0.23\%$. In contrast, the Huangshaping and Tuling granites have higher average SiO_2 but lower average TiO_2 , Al_2O_3 , CaO , total FeO , MgO , MnO and P_2O_5 contents (Fig. 4a–f), with $\text{SiO}_2 = 73.2\text{--}76.9\%$, $\text{TiO}_2 = 0.02\text{--}0.13\%$, $\text{Al}_2\text{O}_3 = 12.2\text{--}13.4\%$, $\text{CaO} = 0.27\text{--}2.3\%$, $\text{FeO} = 0.10\text{--}1.7\%$, $\text{Fe}_2\text{O}_3 = 0.06\text{--}2.2\%$, $\text{MgO} = 0.10\text{--}1.3\%$, $\text{MnO} = 0.01\text{--}0.05\%$ (except one data point of 0.56%) and $\text{P}_2\text{O}_5 = 0.01\text{--}0.04\%$. All of these granitoids are relatively high in total alkalis, with $\text{K}_2\text{O} = 3.2\text{--}8.3\%$ and

$\text{Na}_2\text{O} = 0.26\text{--}3.9\%$, and total $\text{K}_2\text{O} + \text{Na}_2\text{O}$ ranging from 3.4% to 8.9%. In an ANOR-Q' diagram (Fig. 5a), the rocks plot at the boundary of monzogranite and syenogranite, and the Huangshaping and Tuling granites show greater affiliation to monzogranite. In a SiO_2 vs. $\text{K}_2\text{O} + \text{Na}_2\text{O}$ diagram (Fig. 5b), all rocks fall in the sub-alkaline field. The Baoshan and Tongshanling granodiorites plot in the granodiorite field whereas the Huangshaping and Tuling granites plot in the granite field. The A/NK values are also different for these two groups: 1.5–2.5 for the Baoshan and Tongshanling granodiorites; and 1.0–1.5 for the Huangshaping and Tuling granites. The A/CNK values of all rocks range from 0.86 to 1.8, indicating a metaluminous to peraluminous composition (Fig. 5c). All of these rocks are K_2O -rich and thus fall in the fields of high-K granite and shoshonite, with larger variations for the Huangshaping and Tuling granites (Fig. 5d).

The trace elements of these granitic rocks also have varied concentrations and can be grouped into two types (Table 1). Compared to the Baoshan and Tongshanling granodiorites, the Huangshaping and Tuling granites show more fluctuating values and higher average contents of Rb, Th, U, Ga, Hf, Y, Sm, Gd, Dy, Er, Ho, Yb and Lu. In contrast, lower average values are found for the elements Ba, Sr, P, Ti and Eu in the Huangshaping and Tuling granites. On a primitive mantle-normalized multi-element diagram (Fig. 6a), the Baoshan and Tongshanling

Table 1

Major and trace element analyses for the granitic rocks in the South Hunan region.

Granitic pluton	Baoshan						Huangshaping					
Rock type	Porphyritic granodiorite					Granodiorite porphyry	Quartz porphyry		Granophyre			
Sample No.	917-6	917-9	918-10	919-7	919-9	914-7	917-3	923-1	923-4	923-6	923-7	923-10
SiO ₂ (wt. %)	65.98	67.42	65.54	70.25	70.99	68.68	66.30	76.89	73.84	74.87	75.74	73.49
TiO ₂	0.46	0.47	0.46	0.29	0.28	0.37	0.51	0.09	0.08	0.13	0.05	0.19
Al ₂ O ₃	14.74	14.75	15.44	13.73	13.83	14.12	14.81	12.48	12.83	12.43	12.63	12.91
FeO	1.80	2.10	1.82	1.43	1.53	1.85	2.60	0.33	0.65	0.75	0.37	1.03
Fe ₂ O ₃	0.88	1.02	1.25	0.98	0.81	1.15	1.10	0.13	0.88	0.11	0.09	0.17
MgO	1.80	2.10	1.82	1.43	1.53	1.85	2.60	0.33	0.65	0.75	0.37	1.03
CaO	3.79	2.65	4.07	2.24	1.62	1.88	2.47	0.27	1.69	2.00	1.33	2.29
MnO	0.17	0.08	0.09	0.08	0.07	0.09	0.10	0.01	0.02	0.02	0.01	0.03
Na ₂ O	0.51	0.54	0.20	1.62	1.46	0.60	0.72	0.27	0.26	3.43	3.26	3.64
K ₂ O	3.32	3.67	0.80	4.90	5.05	5.20	4.41	8.29	3.18	4.82	5.57	4.55
P ₂ O ₅	0.17	0.19	0.19	0.10	0.09	0.16	0.19	0.01	0.01	0.01	0.01	0.03
LOI	3.94	3.68	5.35	1.89	2.01	2.69	3.23	0.81	3.08	0.47	0.34	0.45
Total	99.84	99.82	99.82	98.94	99.27	98.64	99.04	99.91	97.17	99.79	99.77	99.81
Na ₂ O + K ₂ O	3.83	4.21	1.00	6.52	6.51	5.80	5.13	8.56	3.44	8.25	8.83	8.19
K ₂ O/Na ₂ O	6.51	6.80	4.00	3.02	3.46	8.67	6.13	30.70	12.23	1.41	1.71	1.25
Al ₂ O ₃ /TiO ₂	32	31	34	47	49	38	29	139	160	96	253	68
CaO/Na ₂ O	7.4	4.9	20.4	1.4	1.1	3.1	3.4	1.0	6.5	0.58	0.41	0.63
A/CNK	1.30	1.52	1.79	1.14	1.28	1.40	1.41	1.26	1.84	0.86	0.91	0.86
Rb (ppm)	131	149	17.7	213	215	389	186	541	212	289	442	305
Sr	113	96	155	157	140	139	91	50.1	21.1	57.7	37.7	91.6
Ba	571	615	389	515	496	930	713	86.2	52.4	81.8	54.8	93.9
Ga	19.4	18.1	18.8	16.2	16.5	19.4	17.9	21.9	20.0	22.1	22.8	21.7
Y	24.7	19.5	27.8	16.2	21.9	16.5	19.1	41.2	27.1	46.5	54.0	45.7
Zr	127	139	171	103	107	193	142	105	117	109	108	136
Hf	4.2	4.7	5.9	4.0	4.2	6.1	4.8	4.0	4.4	4.1	4.1	5.0
Nb	26.0	27.9	22.7	18.4	19.1	44.6	26.5	17.4	32.7	25.4	27.0	23.3
Ta	2.03	1.58	1.93	1.77	1.97	3.48	1.59	5.87	4.38	6.08	8.26	5.40
Th	16.0	16.9	15.8	15.6	15.9	27.5	15.4	37.6	37.9	42.3	52.6	39.8
U	4.95	3.00	3.89	4.92	6.38	9.28	3.26	23.7	11.8	16.8	22.3	15.5
Nb/Ta	12.8	17.7	11.8	10.4	9.7	12.8	16.7	3.0	7.5	4.2	3.3	4.3
Zr/Hf	30.2	29.6	29.0	25.8	25.5	31.6	29.6	26.3	26.6	26.69	26.3	27.2
Th/U	3.23	5.63	4.06	3.17	2.49	2.96	4.72	1.59	3.21	2.52	2.36	2.57
La	28.0	30.0	21.9	19.3	21.6	61.9	28.0	12.9	33.3	21.5	21.8	19.8
Ce	55.9	58.7	44.7	38.3	42.1	115	55.3	30.4	68.6	47.0	53.9	44.3
Pr	6.85	7.41	5.75	4.80	5.05	12.7	6.87	4.29	8.65	6.31	6.82	5.86
Nd	26.0	27.9	22.7	18.4	19.1	44.6	26.5	17.4	32.7	25.4	27.0	23.3
Sm	5.62	5.41	5.06	3.93	3.71	7.13	5.20	5.36	7.22	7.35	8.22	7.12
Eu	1.30	1.19	1.23	1.04	0.91	1.22	1.17	0.13	0.33	0.15	0.11	0.28
Gd	4.92	4.57	4.05	3.18	2.92	5.99	4.32	5.22	6.03	6.84	7.54	5.89
Tb	0.83	0.74	0.75	0.56	0.51	0.81	0.72	1.10	1.00	1.33	1.56	1.25
Dy	4.47	3.78	4.16	3.09	2.69	3.34	3.64	7.31	5.08	8.43	9.91	7.77
Ho	0.86	0.75	0.82	0.62	0.53	0.59	0.70	1.48	0.96	1.67	2.00	1.59
Er	2.64	2.29	2.44	1.92	1.78	1.87	2.05	4.32	2.88	4.79	5.75	4.48
Tm	0.40	0.36	0.48	0.27	0.39	0.25	0.35	0.74	0.48	0.83	0.97	0.77
Yb	2.86	2.77	3.18	1.83	2.86	1.81	2.35	5.15	3.40	5.80	6.74	5.29
Lu	0.40	0.39	0.45	0.25	0.41	0.26	0.34	0.69	0.47	0.79	0.89	0.72
ΣREE	141.1	146.3	117.7	97.5	104.6	257.5	137.5	96.5	171.1	138.2	153.2	128.4
LREE/HREE	7.1	8.4	6.2	7.3	7.7	16.3	8.5	2.7	7.4	3.5	3.3	3.6
Eu/Eu*	0.74	0.71	0.80	0.87	0.82	0.56	0.73	0.07	0.15	0.06	0.04	0.13

Granitic pluton	Hangshaping					Tongshanling				Tuling	
Rock type	Granophyre		Granite porphyry			Porphyritic granodiorite				Granite porphyry	
Sample No.	923-14	923-23	925-19	925-26	925-23	TIII728-1	T729-2	TSL1	TSL2	D728-5	TL
SiO ₂ (wt. %)	74.93	76.49	76.33	75.86	75.43	64.50	66.61	66.68	66.15	73.20	73.25
TiO ₂	0.05	0.09	0.02	0.02	0.02	0.60	0.43	0.49	0.46	0.02	0.08
Al ₂ O ₃	12.16	12.84	12.86	12.98	13.09	15.32	15.50	14.78	15.52	13.40	12.95
FeO	0.22	0.10	0.50	1.20	1.25	3.69	2.50	4.65*	3.25*	0.55	1.74
Fe ₂ O ₃	0.16	0.41	0.06	0.12	0.06	0.75	1.03			0.30	2.23
MgO	0.22	0.10	0.50	1.20	1.25	1.90	1.25	1.59	1.75	0.55	0.17
CaO	1.74	0.39	0.67	0.76	0.68	4.34	3.40	2.98	4.20	0.81	1.12
MnO	0.02	0.01	0.02	0.05	0.04	0.07	0.07	0.10	0.05	0.05	0.56
Na ₂ O	2.54	1.00	4.17	3.83	3.87	2.64	3.12	2.58	3.10	0.56	1.43
K ₂ O	6.24	6.95	4.67	4.44	4.52	3.54	4.20	3.60	3.96	8.31	5.12
P ₂ O ₅	0.01	0.01	0.01	0.01	0.01	0.23	0.17	0.21	0.17	0.01	0.04
LOI	0.54	1.06	0.35	0.50	0.65	1.70	1.19	2.38	1.36	1.32	1.32
Total	98.83	99.45	100.16	100.97	100.87	99.28	99.47	99.98	99.95	99.08	100.01
Na ₂ O + K ₂ O	8.78	7.95	8.84	8.27	8.39	6.18	7.32	6.18	7.06	8.87	6.55
K ₂ O/Na ₂ O	2.46	6.95	1.12	1.16	1.17	1.34	1.35	1.40	1.28	14.84	3.58
Al ₂ O ₃ /TiO ₂	243	143	643	649	655	25.5	36.1	30.2	33.7	670	162

(continued on next page)

Table 1 (continued)

Granitic pluton	Hangshaping			Tongshanling				Tuling	
Rock type	Granophyre		Granite porphyry	Porphyritic granodiorite				Granite porphyry	
CaO/Na ₂ O	0.7	0.4	0.2	0.2	0.2	1.6	1.1	1.2	1.4
A/CNK	0.86	1.30	0.98	1.04	1.05	0.95	0.98	1.09	0.91
Rb (ppm)	506	395	538	1097	1018	153	191	170	174
Sr	46.1	60.4	11.8	12.9	16.1	399	402	293	306
Ba	118	91.7	35.6	57.6	36.2	803	912	655	614
Ga	22.8	22.6	27.8	30.1	29.8	19.0	18.4		
Y	48.7	64.1	119	134	129	24.5	16.6	21.2	21.5
Zr	106	124	94.1	110	106	153	217	133	118
Hf	4.00	4.60	4.00	4.00	4.70	4.88	6.06	4.62	3.96
Nb	25.2	53.2	24.6	30.3	30.9	29.6	24.8	17.4	16.5
Ta	7.43	6.78	15.8	18.3	16.8	2.11	1.58	1.78	1.70
Th	40.8	36.7	20.3	30.5	28.6	17.7	13.4	15.2	16.7
U	21.0	19.7	28.7	33.6	30.4	5.10	3.75	5.10	5.76
Nb/Ta	3.39	7.85	1.56	1.66	1.84	14.0	15.7	9.75	9.73
Zr/Hf	26.5	27.0	23.5	27.5	22.6	31.4	35.9	28.7	29.8
Th/U	1.9	1.9	0.71	0.91	0.94	3.5	3.6	3.0	2.9
La	18.7	42.8	13.7	18.7	20.0	35.7	31.9	26.3	31.5
Ce	43.0	102	34.2	46.0	50.4	66.5	57.8	52.1	58.9
Pr	6.09	14.00	5.49	7.01	7.47	7.92	6.77	6.26	7.03
Nd	25.2	53.2	24.6	30.3	30.9	29.6	24.8	23.4	25.1
Sm	7.66	13.1	11.0	12.4	12.5	5.81	4.63	4.56	4.91
Eu	0.06	0.15	0.03	0.03	0.03	1.31	1.28	1.08	1.18
Gd	7.51	11.9	11.4	12.2	12.4	5.19	3.85	3.90	4.36
Tb	1.42	2.09	2.54	2.83	2.83	0.75	0.55	0.63	0.63
Dy	8.92	12.30	18.3	20.2	19.5	4.24	3.05	3.60	3.82
Ho	1.79	2.39	3.74	4.13	3.89	0.81	0.57	0.70	0.77
Er	5.23	6.71	10.8	12.0	11.6	2.30	1.64	2.04	2.30
Tm	0.90	1.06	2.05	2.30	2.14	0.37	0.25	0.32	0.34
Yb	6.28	6.90	14.1	16.1	14.9	2.49	1.70	2.08	2.28
Lu	0.88	0.85	1.93	2.20	2.03	0.37	0.25	0.31	0.34
Σ REE	133.6	269.5	153.9	186.4	190.6	163.3	139.0	127.3	143.5
LREE/HREE	3.06	5.10	1.37	1.59	1.75	8.88	10.72	8.37	8.67
Eu/Eu*	0.02	0.04	0.01	0.01	0.01	0.72	0.90	0.77	0.76
								0.01	0.11

Note: Eu/Eu* = Eu_N/[(Sm_N)(Gd_N)^{1/2}]; figures with a “*” are total FeO; FeO* = FeO + 0.9Fe₂O₃. Samples TSL1 and TSL2 from the Tongshanling pluton are average values reported in Wei et al. (2007) and Wang et al. (2001), respectively. Sample TL from the Tuling pluton is average value reported in GSSH (2008).

granodiorites are characterized by relatively flat patterns, whereas the Huangshaping and Tuling granites exhibit the most obvious anomalies, occupying the peaks and troughs on the diagram. On a chondrite-normalized REE diagram (Fig. 6b), these two groups also show distinct

characteristics. The Baoshan and Tongshanling granodiorites are characterized by visible fractionation of light rare earth elements (LREE) and heavy rare earth elements (HREE), with slight negative Eu anomalies (Eu/Eu* = 0.56–0.90). In contrast, the Huangshaping and

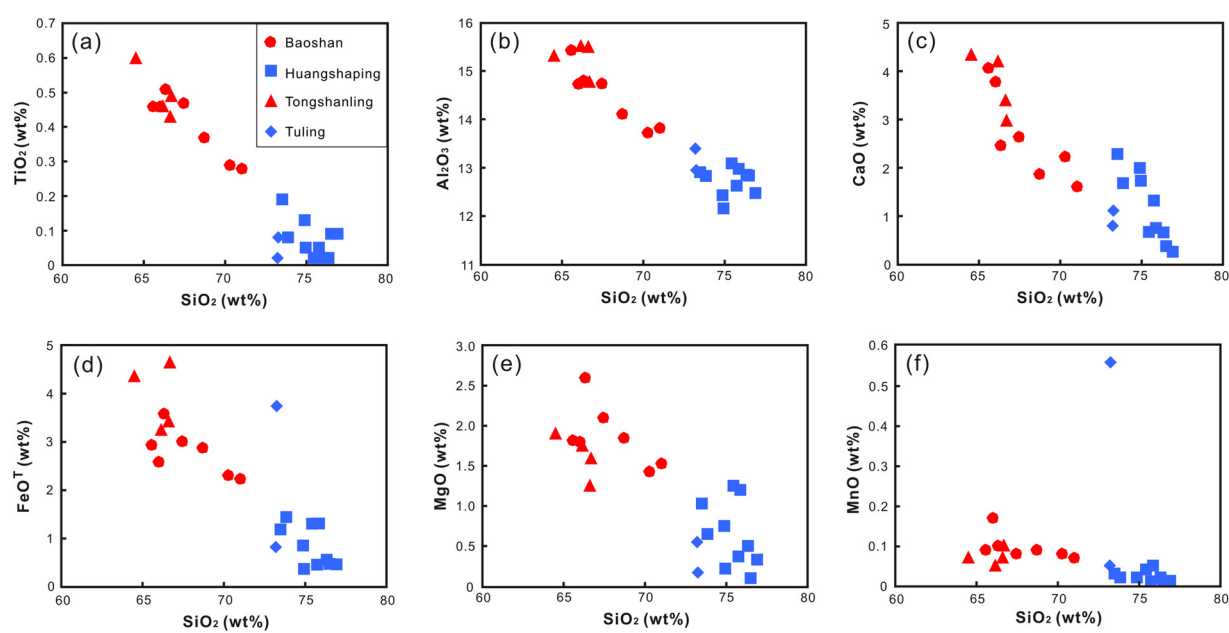


Fig. 4. Harker diagrams illustrating major elemental variations of the granitic rocks from South Hunan. (a) SiO₂ vs. TiO₂; (b) SiO₂ vs. Al₂O₃; (c) SiO₂ vs. CaO; (d) SiO₂ vs. FeO^T; (e) SiO₂ vs. MgO; (f) SiO₂ vs. MnO.

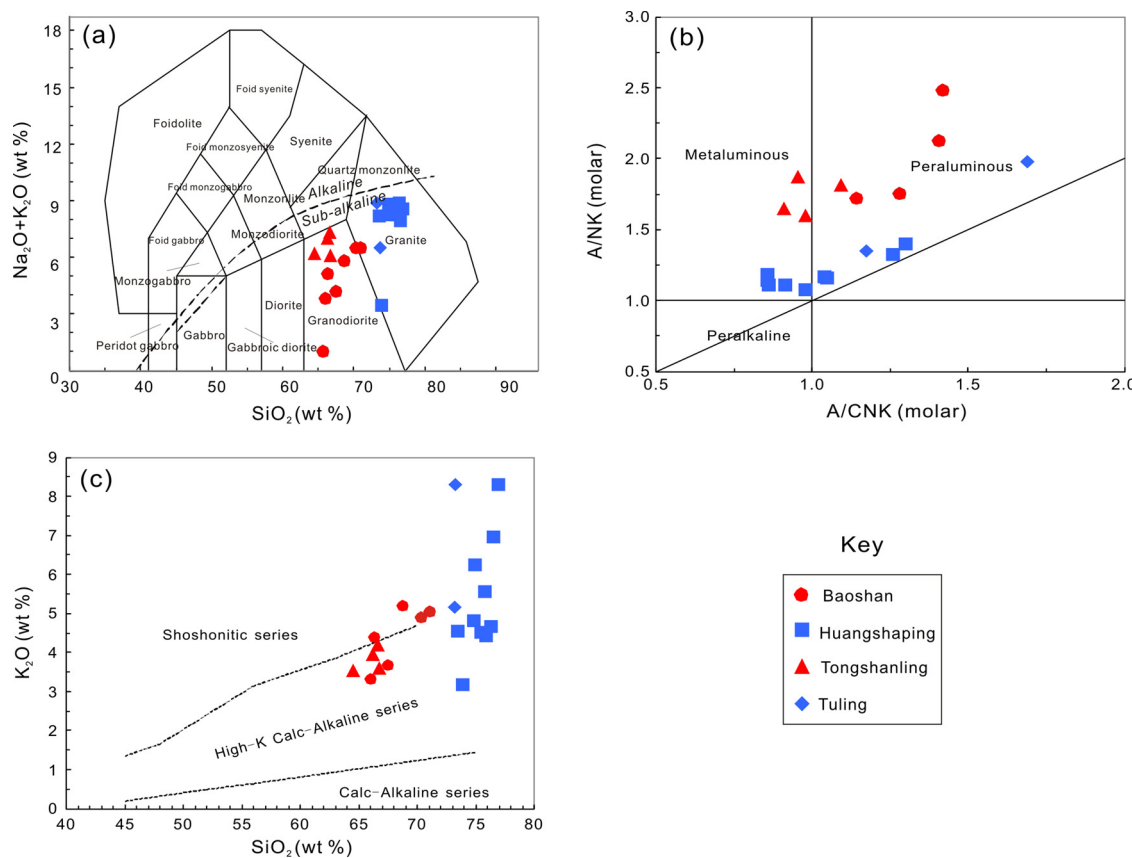


Fig. 5. Discrimination diagrams for granitic rocks from South Hunan. (a) SiO_2 vs. $(\text{K}_2\text{O} + \text{Na}_2\text{O})$ diagram (after Le Bas et al., 1986 and Le Maitre, 1989); (b) A/KNC diagram, where $\text{A}/\text{KNC} = \text{Al}_2\text{O}_3$ (molar)/ $(\text{K}_2\text{O} + \text{Na}_2\text{O} + \text{CaO})$ (molar), $\text{A}/\text{NK} = \text{Al}_2\text{O}_3$ (molar)/ $(\text{Na}_2\text{O} + \text{K}_2\text{O})$ (after Frost et al., 2001); (c) SiO_2 vs. K_2O diagram (after Wheller et al., 1987).

Tuling granites are characterized by enrichment of HREE, relatively flat REE patterns and visible lanthanide tetrad effects, with pronounced negative Eu anomalies ($\text{Eu}/\text{Eu}^* = 0.01\text{--}0.15$).

4.2. Zircon morphology and U-Pb geochronology

Typical CL images of the zircons are shown in Fig. 7. Most of the zircon grains have internal oscillatory zonation, suggesting a typical magmatic origin (Hoskin and Schaltegger, 2003; Li et al., 2017b, 2018d, 2018e; Sun et al., 2017a). Moreover, these zircon crystals can be

grouped into two types based on their length-to-width ratios. Zircons from the Baoshan and Tongshanling granodiorites are shaped like long prisms, with lengths ranging from 200 μm to 400 μm , and length-to-width ratios ranging from 2:1 to 4:1. In contrast, zircons from the Huangshaping and Tuling granites have short columnar shapes, with lengths ranging from 80 μm to 200 μm , and length-to-width ratios ranging from 1:1 to 2:1.

The LA-ICPMS analytical results for U-Pb dating of zircons in the granitic rocks are shown in Table 2. After excluding results of very old age (≥ 800 Ma, considered to be inherited zircons) and unreliable data

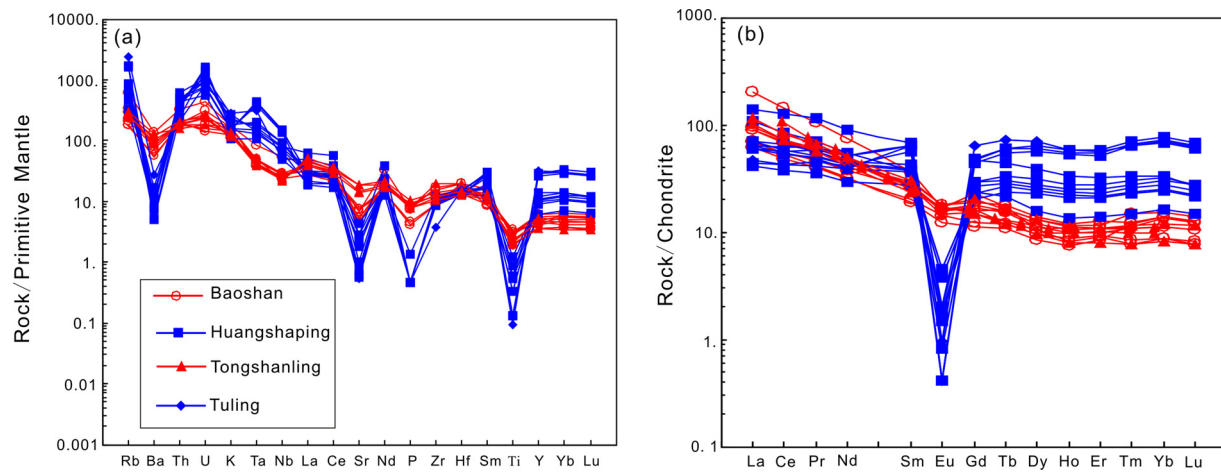


Fig. 6. (a) Primitive mantle-normalized trace element and (b) chondrite-normalized REE patterns for the granitic rocks in South Hunan. Normalized values for primitive mantle and chondrite are from Sun and McDonough (1989), and Taylor and McLennan (1985), respectively.

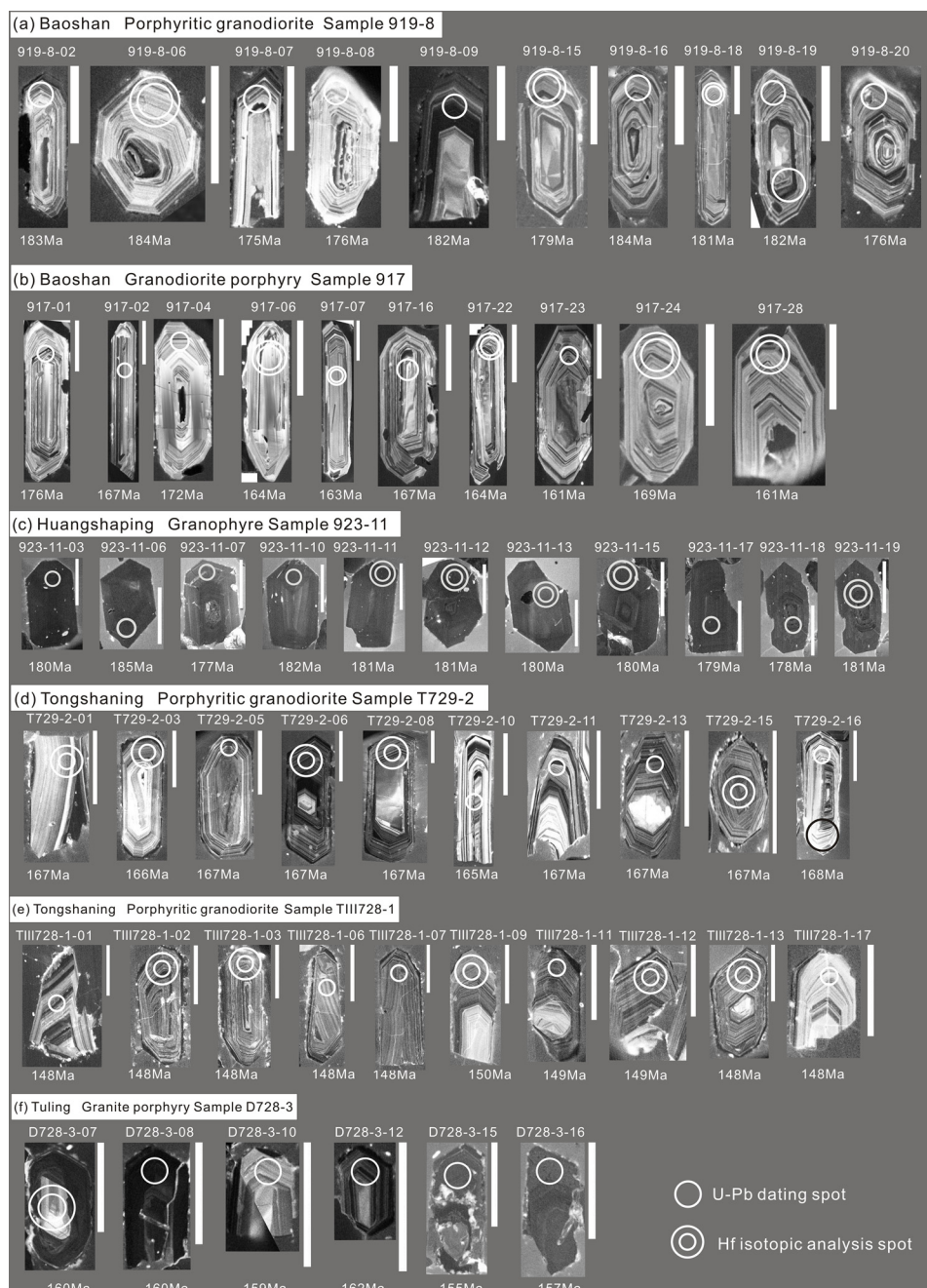


Fig. 7. CL images of zircon grains from the granitic rocks in the (a–b) Baoshan, (c) Huangshaping, (d–e) Tongshanling and (f) Tuling areas. Length of the white bar scale is 100 μm .

(concordance < 90%), 70 reliable age dates were obtained with $^{206}\text{Pb}/^{238}\text{U}$ ages ranging from 147.5 to 186 Ma.

The $^{206}\text{Pb}/^{238}\text{U}$ ages of 15 zircon grains of sample 919-8 from the Baoshan pluton range from 175 Ma to 186 Ma, and plot on or close to the concordia curve, with a weighted mean $^{206}\text{Pb}/^{238}\text{U}$ age of 180.5 ± 1.6 Ma (MSWD = 1.5; Fig. 8a), which is regarded as the crystallization age of the porphyritic granodiorite. By contrast, 17 zircons of the granodiorite porphyry (sample 917) from the Baoshan pluton have $^{206}\text{Pb}/^{238}\text{U}$ ages ranging from 156 Ma to 179 Ma and yield a concordant U–Pb age of 167.0 ± 3.0 (MSWD = 1.12, Fig. 8b). For the Huangshaping granite, the $^{206}\text{Pb}/^{238}\text{U}$ ages of 11 zircon grains from the granophyre (sample 923-11) range from 177 Ma to 185 Ma, with a concordant U–Pb age of 180.0 ± 1.0 (MSWD = 1.0, Fig. 8c). This granite is younger than the quartz porphyry of the first intrusive phase (~189 Ma, Li et al., 2014a) but older than the granite porphyry of the

third phase (160–155 Ma, Yuan et al., 2014). The two granodiorite samples from the Tongshanling area have different U–Pb ages. Sample T729-2 from intrusion I has a narrow $^{206}\text{Pb}/^{238}\text{U}$ age interval ranging from 165 Ma to 168 Ma, and data plot on or close to the concordia curve with a concordant U–Pb age of 166.6 ± 0.4 Ma (MSWD = 0.23; Fig. 8d). The other sample (TIII728-1) taken from intrusion III has younger $^{206}\text{Pb}/^{238}\text{U}$ ages ranging from 147.5 Ma to 150 Ma, with a concordant U–Pb age of 148.3 ± 0.5 Ma (MSWD = 0.5, Fig. 8e). Zircons of the granite porphyry (sample D728-3) from the Tuling area are characterized by varied $^{206}\text{Pb}/^{238}\text{U}$ ages and large discordance. Only 6 spots from this sample yielded reliable $^{206}\text{Pb}/^{238}\text{U}$ ages ranging from 154.9 Ma to 160 Ma, with a concordant U–Pb age of 158.7 ± 2.3 Ma (MSWD = 0.78, Fig. 8f).

Table 2

LA-ICPMS zircon U-Pb dating results for the granitic rocks in the South Hunan region.

Spots No.	Isotope ratio						Apparent age (Ma)					
	$^{207}\text{Pb}/^{206}\text{Pb} \pm 1\sigma$		$^{207}\text{Pb}/^{235}\text{U} \pm 1\sigma$		$^{206}\text{Pb}/^{238}\text{U} \pm 1\sigma$		$^{207}\text{Pb}/^{206}\text{Pb} \pm 1\sigma$		$^{207}\text{Pb}/^{235}\text{U} \pm 1\sigma$		$^{206}\text{Pb}/^{238}\text{U} \pm 1\sigma$	
<i>Baoshan pluton Porphyritic granodiorite Sample 919-8</i>												
919-8-01	0.04834	0.00265	0.19283	0.01230	0.02920	0.00057	116	106	179	10	186	4
919-8-02	0.04670	0.00227	0.18541	0.01122	0.02887	0.00048	34	100	173	10	183	3
919-8-03	0.05229	0.00588	0.20851	0.02281	0.02892	0.00075	298	258	192	19	184	5
919-8-06	0.05064	0.00421	0.20205	0.01643	0.02894	0.00050	225	190	187	14	184	3
919-8-07	0.04768	0.00237	0.18084	0.01161	0.02752	0.00048	84	110	169	10	175	3
919-8-08	0.04996	0.00286	0.19032	0.01317	0.02760	0.00043	193	129	177	11	176	3
919-8-09	0.04782	0.00172	0.18896	0.01005	0.02856	0.00040	91	92	176	9	182	3
919-8-12	0.05557	0.00292	0.22311	0.01434	0.02928	0.00049	435	114	204	12	186	3
919-8-13	0.04343	0.00267	0.17056	0.01216	0.02861	0.00054	100	121	160	11	182	3
919-8-15	0.05451	0.00189	0.21278	0.01050	0.02810	0.00037	392	87	196	9	179	2
919-8-16	0.05431	0.00238	0.21624	0.01107	0.02895	0.00066	384	74	199	9	184	4
919-8-17	0.05007	0.00501	0.19753	0.01908	0.02861	0.00075	198	228	183	16	182	5
919-8-18	0.04858	0.00296	0.19034	0.01251	0.02847	0.00056	128	111	177	11	181	4
919-8-19	0.05346	0.00254	0.21195	0.01179	0.02869	0.00051	348	93	195	10	182	3
919-8-20	0.05337	0.00212	0.20311	0.00912	0.02763	0.00035	345	79	188	8	176	2
<i>Baoshan pluton Granodiorite porphyry Sample 917</i>												
917-01	0.05294	0.00244	0.20077	0.01030	0.02763	0.00050	326	84	186	9	176	3
917-02	0.05039	0.00355	0.18287	0.01261	0.02632	0.00039	213	161	171	11	167	2
917-04	0.05655	0.00604	0.21107	0.02170	0.02707	0.00078	474	243	194	18	172	5
917-06	0.05325	0.00292	0.18939	0.00996	0.02581	0.00048	339	85	176	9	164	3
917-07	0.04977	0.00300	0.17555	0.01016	0.02558	0.00044	184	138	164	9	163	3
917-15	0.04996	0.00234	0.18151	0.00912	0.02645	0.00049	193	82	169	8	168	3
917-16	0.05924	0.00245	0.21190	0.00954	0.02624	0.00071	576	53	195	8	167	4
917-17	0.04896	0.00316	0.17893	0.01119	0.02650	0.00041	146	146	167	10	169	3
917-18	0.04993	0.00361	0.19386	0.01353	0.02816	0.00052	192	165	180	12	179	3
917-21	0.05202	0.00250	0.19022	0.00950	0.02646	0.00050	286	79	177	8	168	3
917-22	0.04994	0.00169	0.17788	0.00749	0.02582	0.00032	192	75	166	6	164	2
917-23	0.05183	0.00229	0.18006	0.00915	0.02522	0.00032	278	93	168	8	161	2
917-24	0.05034	0.00232	0.18408	0.00978	0.02660	0.00040	211	95	172	8	169	3
917-25	0.05073	0.00279	0.19322	0.01146	0.02778	0.00051	228	103	179	10	177	3
917-26	0.05321	0.00363	0.18007	0.01196	0.02455	0.00038	338	158	168	10	156	2
917-28	0.05420	0.00273	0.18863	0.01011	0.02522	0.00038	379	94	175	9	161	2
917-29	0.05151	0.00276	0.17500	0.00944	0.02469	0.00042	264	93	164	8	157	3
<i>Huangshaping pluton Granophyre Sample 923-11</i>												
923-11-03	0.05140	0.00054	0.20044	0.00262	0.02828	0.00029	259	14	185	2	180	2
923-11-06	0.04965	0.00068	0.20011	0.00342	0.02917	0.00036	179	19	185	3	185	2
923-11-07	0.05302	0.00067	0.20384	0.00268	0.02783	0.00022	330	16	188	2	177	1
923-11-10	0.04976	0.00056	0.19677	0.00311	0.02865	0.00032	184	18	182	3	182	2
923-11-11	0.04940	0.00046	0.19410	0.00251	0.02850	0.00025	167	15	180	2	181	2
923-11-12	0.04926	0.00041	0.19313	0.00256	0.02842	0.00022	160	17	179	2	181	1
923-11-13	0.04872	0.00039	0.19066	0.00253	0.02832	0.00018	134	19	177	2	180	1
923-11-15	0.05089	0.00043	0.19911	0.00246	0.02832	0.00021	236	15	184	2	180	1
923-11-17	0.04922	0.00036	0.19203	0.00258	0.02818	0.00024	158	16	178	2	179	2
923-11-18	0.05080	0.00043	0.19629	0.00279	0.02804	0.00034	232	15	182	2	178	2
923-11-19	0.04991	0.00044	0.19539	0.00258	0.02845	0.00033	191	14	181	2	181	2
<i>Tongshan pluton Porphyritic granodiorite Sample T729-2</i>												
T729-2-01	0.04995	0.00093	0.18253	0.00477	0.02621	0.00027	192	41	170	4	167	2
T729-2-03	0.04832	0.00106	0.17476	0.00463	0.02611	0.00022	115	47	164	4	166	1
T729-2-04	0.05120	0.00151	0.18598	0.00695	0.02618	0.00039	250	58	173	6	167	2
T729-2-05	0.04959	0.00087	0.18023	0.00460	0.02621	0.00024	176	42	168	4	167	2
T729-2-06	0.04850	0.00095	0.17581	0.00478	0.02621	0.00019	124	50	164	4	167	1
T729-2-08	0.04915	0.00093	0.17926	0.00479	0.02618	0.00017	155	50	167	4	167	1
T729-2-10	0.05085	0.00158	0.18183	0.00546	0.02594	0.00020	234	73	170	5	165	1
T729-2-11	0.05178	0.00131	0.18721	0.00455	0.02622	0.00018	276	59	174	4	167	1
T729-2-13	0.05071	0.00129	0.18348	0.00448	0.02624	0.00019	228	60	171	4	167	1
T729-2-15	0.04876	0.00102	0.17738	0.00409	0.02619	0.00017	136	42	166	4	167	1
T729-2-16	0.05032	0.00148	0.18290	0.00552	0.02636	0.00023	210	54	171	5	168	1
<i>Tongshan pluton Porphyritic granodiorite Sample TIII728-1</i>												
TIII728-1-01	0.04965	0.00167	0.15916	0.00523	0.02325	0.00016	179	80	150	5	148	1
TIII728-1-02	0.05022	0.00083	0.16022	0.00404	0.02314	0.00014	205	48	151	4	147.5	0.9
TIII728-1-03	0.04960	0.00092	0.15819	0.00380	0.02317	0.00014	176	45	149	3	147.7	0.9
TIII728-1-06	0.05231	0.00168	0.16701	0.00495	0.02316	0.00029	299	75	157	4	148	2
TIII728-1-07	0.04869	0.00100	0.15602	0.00353	0.02329	0.00017	133	39	147	3	148	1
TIII728-1-09	0.05168	0.00089	0.16771	0.00340	0.02352	0.00018	271	32	157	3	150	1
TIII728-1-11	0.05202	0.00103	0.16803	0.00419	0.02336	0.00025	286	38	158	4	149	2
TIII728-1-12	0.05068	0.00096	0.16381	0.00392	0.02337	0.00019	226	40	154	3	149	1
TIII728-1-13	0.05054	0.00111	0.16279	0.00431	0.02327	0.00015	220	49	153	4	148.3	1
TIII728-1-17	0.05064	0.00190	0.16199	0.00594	0.02320	0.00019	225	89	152	5	148	1
<i>Tuling pluton Granite porphyry Sample D728-3</i>												

(continued on next page)

Table 2 (continued)

Spots No.	Isotope ratio			Apparent age (Ma)		
	$^{207}\text{Pb}/^{206}\text{Pb} \pm 1\sigma$	$^{207}\text{Pb}/^{235}\text{U} \pm 1\sigma$	$^{206}\text{Pb}/^{238}\text{U} \pm 1\sigma$	$^{207}\text{Pb}/^{206}\text{Pb} \pm 1\sigma$	$^{207}\text{Pb}/^{235}\text{U} \pm 1\sigma$	$^{206}\text{Pb}/^{238}\text{U} \pm 1\sigma$
D728-3-07	0.04942	0.00081	0.17154	0.00285	0.02508	0.00023
D728-3-08	0.05084	0.00197	0.17611	0.00648	0.02512	0.00031
D728-3-10	0.05316	0.00196	0.18262	0.00664	0.02497	0.00026
D728-3-12	0.04927	0.00102	0.17266	0.00339	0.02542	0.00016
D728-3-15	0.05385	0.00093	0.18060	0.00295	0.02433	0.00013
D728-3-16	0.05395	0.00074	0.18372	0.00235	0.02470	0.00013
				168	22	161
				234	92	165
				336	63	170
				161	49	162
				365	40	169
				369	32	171
						157.3
						0.8

4.3. Zircon Hf isotopes

The zircon Hf isotopic results and age model parameters for the granitic rocks in the study areas are shown in Table 3.

Granitic rocks from the Baoshan pluton have similar zircon Hf isotopic characteristics. Five zircon grains of the porphyritic granodiorite (sample 919-8) have varied $^{176}\text{Yb}/^{177}\text{Hf}$ (0.022333–0.038398) and $^{176}\text{Lu}/^{177}\text{Hf}$ (0.001022–0.001611) ratios, with initial $^{176}\text{Hf}/^{177}\text{Hf}$ and $\epsilon\text{Hf(t)}$ values ranging from 0.282336 to 0.282379 and from -9.86 to -11.48, respectively. Single-stage model ages (T_{DM1}) range from 1229 Ma to 1302 Ma and average at 1270 Ma (SD (standard deviation) = 26), with an average crustal model age ($T_{\text{DM}^{\text{C}}}$) of 1951 Ma (SD = 62). Similar to sample 919-8, the granodiorite porphyry (sample 917) also has varied zircon $^{176}\text{Yb}/^{177}\text{Hf}$ and $^{176}\text{Lu}/^{177}\text{Hf}$ ratios, of 0.013774–0.033307 and 0.000624–0.001402, respectively. The initial $^{176}\text{Hf}/^{177}\text{Hf}$ and $\epsilon\text{Hf(t)}$ values of eight zircons in this sample are 0.282408–0.282501 and -5.87 to -9.42, respectively, with slightly younger single-stage model ages (average $T_{\text{DM1}} = 1136$ Ma, SD = 38) and crustal model ages (average $T_{\text{DM}^{\text{C}}} = 1709$ Ma, SD = 66).

The Huangshaping granophyre (sample 923-11) has distinct zircon Hf isotopic features. Seven zircon grains have varied $^{176}\text{Yb}/^{177}\text{Hf}$ (0.071267–0.099985) and $^{176}\text{Lu}/^{177}\text{Hf}$ (0.002714–0.003746) ratios, with initial $^{176}\text{Hf}/^{177}\text{Hf}$ and $\epsilon\text{Hf(t)}$ values ranging from 0.282622 to 0.282774 and from -15.84 to -19.70, respectively. Model ages (T_{DM1}) and crustal model ages ($T_{\text{DM}^{\text{C}}}$) range from 1522 Ma to 1711 Ma

(averaging 1622 Ma, SD = 75) and from 2220 Ma to 2459 Ma (averaging 2347 Ma, SD = 97), respectively. This is different from the third-phase granite porphyry from the Huangshaping pluton, which has much younger T_{DM1} and $T_{\text{DM}^{\text{C}}}$, with average values of 1200 Ma (SD = 68) and 1556 Ma (SD = 72), respectively (Ai, 2013; Yuan et al., 2014).

Two granodiorite samples from the Tongshanling pluton have different zircon Hf isotopic ratios. Six zircon grains of sample T729-2 from intrusion I have $^{176}\text{Yb}/^{177}\text{Hf}$ and $^{176}\text{Lu}/^{177}\text{Hf}$ ratios ranging from 0.025373 to 0.046300 and from 0.001074 to 0.001866, respectively. They are characterized by very low initial $^{176}\text{Hf}/^{177}\text{Hf}$ and large negative $\epsilon\text{Hf(t)}$ values that range from 0.282033 to 0.282223 and from -15.86 to -22.67, respectively, with very old model ages ($T_{\text{DM1}} = 1454$ –1755 Ma, averaging 1603 Ma, SD = 103) and crustal model ages ($T_{\text{DM}^{\text{C}}} = 2220$ –2647 Ma, averaging 2464 Ma, SD = 147). The other sample (TIII728-1) taken from intrusion III has much lower $^{176}\text{Yb}/^{177}\text{Hf}$ (0.022103–0.029529) and $^{176}\text{Lu}/^{177}\text{Hf}$ ratios (0.000957–0.001266), with T_{DM1} and $T_{\text{DM}^{\text{C}}}$ ranging from 1206 Ma to 1246 Ma (averaging 1225 Ma, SD = 14) and from 1841 Ma to 1898 Ma (averaging 1857 Ma, SD = 20), respectively.

Only two zircon grains from the Tuling granite porphyry (sample D728-3) have been analyzed for Hf isotopes. One is an inherited zircon (1251 Ma) and the other one is a magmatic zircon (160 Ma). The former has low $^{176}\text{Yb}/^{177}\text{Hf}$ (0.027348) and $^{176}\text{Lu}/^{177}\text{Hf}$ (0.001067) ratios, while the latter has relatively high $^{176}\text{Yb}/^{177}\text{Hf}$ (0.041256) and $^{176}\text{Lu}/^{177}\text{Hf}$ (0.001743) ratios. They both have low initial $^{176}\text{Hf}/^{177}\text{Hf}$

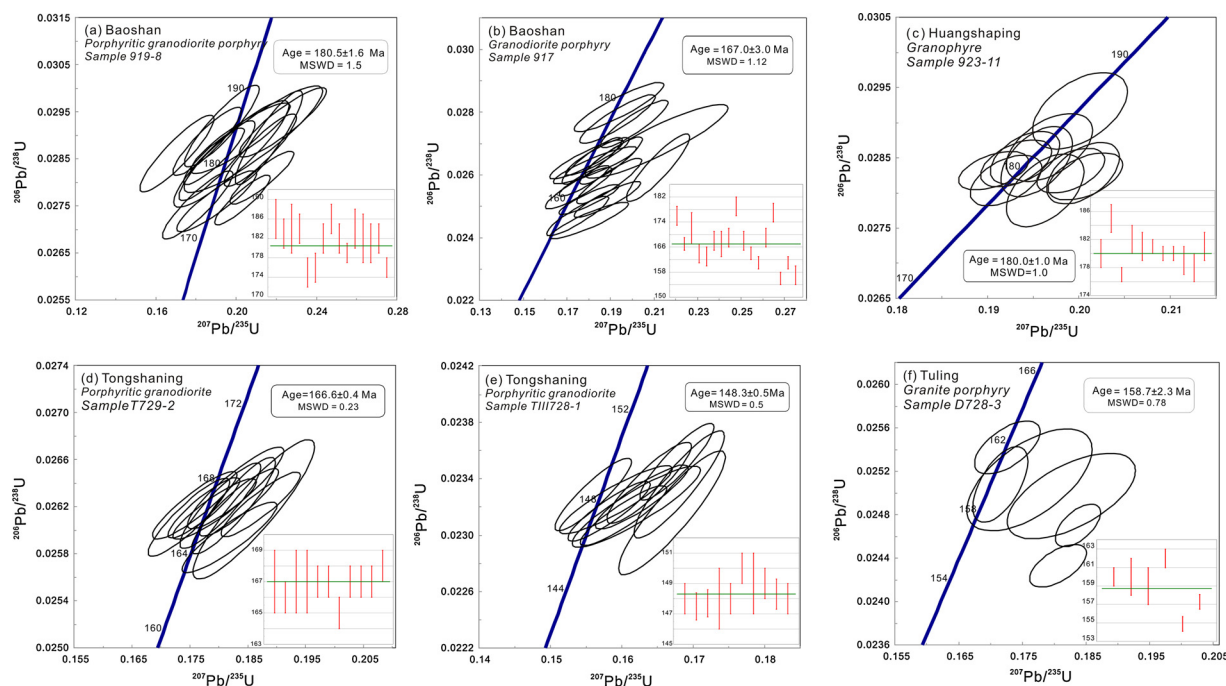


Fig. 8. Zircon U-Pb age dating results for the (a) Baoshan porphyritic granodiorite (sample 919-8), (b) Baoshan granodiorite porphyry (sample 917), (c) Huangshaping granophyre (sample 923-11), (d) Tongshanling porphyritic granodiorite (sample T729-2), (e) Tongshanling porphyritic granodiorite (sample TIII728-1) and (f) Tuling granite porphyry (sample D728-3).

Table 3

LA-MC-ICPMS zircon Hf analytical results for the granitic rocks in the South Hunan region.

Spots No.	$^{176}\text{Hf}/^{177}\text{Hf} \pm 2\sigma$	$^{176}\text{Yb}/^{177}\text{Hf} \pm 2\sigma$	$^{176}\text{Lu}/^{177}\text{Hf} \pm 2\sigma$	T(Ma)	$f_{\text{Lu/Hf}}$	$(^{176}\text{Hf}/^{177}\text{Hf})_i$	$\epsilon_{\text{Hf}}(t)$	$T_{\text{DM1}} (\text{Ma})$	$T_{\text{DM}}^c (\text{Ma})$
<i>Baoshan pluton Porphyritic granodiorite Sample 919-8</i>									
919-8-06	0.282383 ± 0.000017	0.022333 ± 0.000133	0.001022 ± 0.000006	184	-0.97	0.282379	-9.9	1229	1870
919-8-14	0.282350 ± 0.000017	0.024627 ± 0.000184	0.001025 ± 0.000007	172	-0.97	0.282347	-11.3	1274	2061
919-8-15	0.282341 ± 0.000014	0.034277 ± 0.000167	0.001481 ± 0.000006	179	-0.96	0.282336	-11.5	1302	1930
919-8-18	0.282342 ± 0.000014	0.027167 ± 0.000160	0.001176 ± 0.000006	181	-0.96	0.282338	-11.4	1291	1949
919-8-19	0.282378 ± 0.000012	0.038398 ± 0.000346	0.001611 ± 0.000014	182	-0.95	0.282372	-11.2	1255	1947
<i>Baoshan pluton Granodiorite porphyry Sample 917</i>									
917-03	0.282505 ± 0.000010	0.031693 ± 0.000136	0.001337 ± 0.000006	169	-0.96	0.282501	-5.9	1065	1589
917-05	0.282453 ± 0.000012	0.031551 ± 0.000124	0.001345 ± 0.000005	160	-0.96	0.282448	-7.9	1141	1709
917-06	0.282465 ± 0.000014	0.033307 ± 0.000164	0.001402 ± 0.000007	164	-0.96	0.282461	-7.4	1124	1678
917-07	0.282438 ± 0.000015	0.024812 ± 0.000147	0.001085 ± 0.000007	163	-0.97	0.282435	-8.4	1153	1739
917-22	0.282483 ± 0.000015	0.027930 ± 0.000111	0.001180 ± 0.000005	164	-0.96	0.282480	-6.7	1092	1640
917-24	0.282420 ± 0.000018	0.023206 ± 0.000115	0.001050 ± 0.000006	169	-0.97	0.282417	-8.9	1177	1775
917-28	0.282435 ± 0.000017	0.023246 ± 0.000210	0.001044 ± 0.000010	161	-0.97	0.282432	-8.5	1156	1745
917-29	0.282410 ± 0.000017	0.013774 ± 0.000027	0.000624 ± 0.000001	157	-0.98	0.282408	-9.4	1178	1800
<i>Huangshaping pluton Granophyre Sample 923-11</i>									
923-11-01	0.282200 ± 0.000019	0.075913 ± 0.000444	0.002898 ± 0.000015	183	-0.91	0.282622	-16.6	1561	2267
923-11-02	0.282141 ± 0.000021	0.078769 ± 0.000532	0.002944 ± 0.000016	180	-0.91	0.282736	-18.7	1650	2398
923-11-11	0.282221 ± 0.000019	0.071267 ± 0.000428	0.002714 ± 0.000015	181	-0.92	0.282700	-15.8	1522	2220
923-11-12	0.282218 ± 0.000022	0.075203 ± 0.000619	0.002893 ± 0.000023	181	-0.91	0.282722	-16.0	1534	2228
923-11-13	0.282115 ± 0.000019	0.088547 ± 0.000485	0.003442 ± 0.000020	180	-0.9	0.282774	-19.7	1711	2459
923-11-15	0.282127 ± 0.000015	0.099985 ± 0.000386	0.003746 ± 0.000014	180	-0.89	0.282757	-19.3	1708	2435
923-11-19	0.282129 ± 0.000015	0.078594 ± 0.000403	0.002984 ± 0.000015	181	-0.91	0.282710	-19.1	1669	2423
<i>Tongshanling pluton Porphyritic granodiorite Sample T729-2</i>									
T729-2-01	0.282033 ± 0.000018	0.046300 ± 0.000231	0.001866 ± 0.000009	167	-0.94	0.282027	-22.7	1755	2633
T729-2-03	0.282113 ± 0.000018	0.033338 ± 0.000124	0.001387 ± 0.000006	166	-0.96	0.282109	-19.8	1620	2455
T729-2-06	0.282164 ± 0.000017	0.028639 ± 0.000105	0.001200 ± 0.000004	167	-0.96	0.282160	-18.0	1542	2343
T729-2-08	0.282223 ± 0.000018	0.025373 ± 0.000234	0.001074 ± 0.000008	167	-0.97	0.282220	-15.9	1454	2211
T729-2-15	0.282169 ± 0.000019	0.031975 ± 0.000354	0.001413 ± 0.000017	167	-0.96	0.282165	-17.8	1543	2333
T729-2-16	0.282056 ± 0.000017	0.037889 ± 0.000509	0.001526 ± 0.000021	168	-0.95	0.282051	-21.82	1708	2582
<i>Tongshanling pluton Porphyritic granodiorite Sample TIII728-1</i>									
TIII728-1-13	0.282397 ± 0.000016	0.022103 ± 0.000188	0.000957 ± 0.000008	148.3	-0.97	0.282395	-10.1	1206	1835
TIII728-1-12	0.282389 ± 0.000015	0.027677 ± 0.000161	0.001187 ± 0.000006	149	-0.96	0.282386	-10.4	1225	1854
TIII728-1-09	0.282384 ± 0.000015	0.028741 ± 0.000027	0.001187 ± 0.000001	150	-0.96	0.282381	-10.6	1232	1865
TIII728-1-03	0.282372 ± 0.000017	0.026073 ± 0.000026	0.001108 ± 0.000001	147.7	-0.97	0.282369	-11.0	1246	1892
TIII728-1-02	0.282396 ± 0.000013	0.029529 ± 0.000058	0.001266 ± 0.000002	147.5	-0.96	0.282393	-10.2	1217	1840
<i>Tuling pluton Granite porphyry Sample D728-3</i>									
D728-3-05	0.281674 ± 0.000016	0.027348 ± 0.000049	0.001067 ± 0.000002	1251	-0.97	0.281649	-12.0	2215	2816
D728-3-07	0.281878 ± 0.000021	0.041256 ± 0.000552	0.001743 ± 0.000023	160	-0.95	0.281873	-28.3	1968	2974

Note: $(^{176}\text{Hf}/^{177}\text{Hf})_i = (^{176}\text{Hf}/^{177}\text{Hf})_{\text{initial}} = (^{176}\text{Hf}/^{177}\text{Hf})_s - (^{176}\text{Lu}/^{177}\text{Hf})_s \cdot (e^{\lambda t} - 1)$; $\epsilon_{\text{Hf}}(t) = \{[(^{176}\text{Hf}/^{177}\text{Hf})_s - (^{176}\text{Lu}/^{177}\text{Hf})_s] / (^{176}\text{Hf}/^{177}\text{Hf})\}_{\text{CHUR}, 0} - (^{176}\text{Lu}/^{177}\text{Hf})_{\text{CHUR}} \cdot (e^{\lambda t} - 1)\} \cdot 10,000$; $f_{\text{Lu/Hf}} = (^{176}\text{Lu}/^{177}\text{Hf})_s / (^{176}\text{Lu}/^{177}\text{Hf})_{\text{CHUR}} - 1$; $T_{\text{DM}} = 1/\lambda \cdot \ln[1 + (^{176}\text{Hf}/^{177}\text{Hf})_s - (^{176}\text{Hf}/^{177}\text{Hf})_{\text{DM}}] / [(^{176}\text{Lu}/^{177}\text{Hf})_s - (^{176}\text{Lu}/^{177}\text{Hf})_{\text{DM}}]$; $T_{\text{DM}}^c = T_{\text{DM}} - (T_{\text{DM}} - t)[(f_{\text{CC}} - f_{\text{DM}})/(f_{\text{CC}} - f_{\text{DM}})]$. where t is crystal age which dated by zircon analysis; λ is ^{176}Lu β -decay constant; $(^{176}\text{Hf}/^{177}\text{Hf})_i$ is initial $^{176}\text{Hf}/^{177}\text{Hf}$ ratio in samples; $(^{176}\text{Hf}/^{177}\text{Hf})_s$ and $(^{176}\text{Lu}/^{177}\text{Hf})_s$ are values measured in samples; $\epsilon_{\text{Hf}}(t)$ and $f_{\text{Lu/Hf}}$ are deviation of Hf isotopic composition from chondrites; $(^{176}\text{Hf}/^{177}\text{Hf})_{\text{CHUR}, 0}$ and $(^{176}\text{Lu}/^{177}\text{Hf})_{\text{CHUR}}$ are evolution of the $(^{176}\text{Hf}/^{177}\text{Hf})$ and $(^{176}\text{Lu}/^{177}\text{Hf})$ ratios in Chondritic Uniform Reservoir, respectively; $(^{176}\text{Hf}/^{177}\text{Hf})_{\text{DM}}$ and $(^{176}\text{Lu}/^{177}\text{Hf})_{\text{DM}}$ are $(^{176}\text{Hf}/^{177}\text{Hf})$ and $(^{176}\text{Lu}/^{177}\text{Hf})$ ratios in Depleted Mantle (DM), respectively; T_{DM} is single-stage evolutionary Depleted Mantle Hf model age of source rock; T_{DM}^c is Crust model age; f_{CC} , f_{S} and f_{DM} are present $f_{\text{Lu/Hf}}$ values of continental crust, samples and depleted mantle, respectively. $\lambda = 1.867 \times 10^{-11} \text{ yr}^{-1}$ (Patchett and Tatsumoto, 1980); $(^{176}\text{Hf}/^{177}\text{Hf})_{\text{CHUR}, 0} = 0.282772$, $(^{176}\text{Lu}/^{177}\text{Hf})_{\text{CHUR}} = 0.03321$ (Blichert-Toft and Albarède, 1997); $(^{176}\text{Hf}/^{177}\text{Hf})_{\text{DM}} = 0.28325$, $(^{176}\text{Lu}/^{177}\text{Hf})_{\text{DM}} = 0.03824$ (Griffin et al., 2000); $f_{\text{CC}} = -0.55$ (average crust, Griffin et al., 2002); $f_{\text{DM}} = -0.1566$ (Griffin et al., 2000).

ratios (0.281648–0.281873), with distinctively old T_{DM1} (1968–2215 Ma) and T_{DM}^c (2816–2974 Ma).

5. Discussion

5.1. Classification, magmatic evolution and tectonic setting of the granites

In the southern Hunan Province, two types of granites can be readily distinguished based on their mineralogical and geochemical characteristics. The Baoshan and Tongshanling granodiorites commonly contain hornblende and are characterized by flat patterns on primitive-mantle-normalized multi-element diagrams and chondrite-normalized REE diagrams. In contrast, the Huangshaping and Tuling granites are enriched in Rb, U and Th but are significantly depleted in Ba, Sr, Ti and P, with strong negative Eu anomalies in chondrite-normalized REE patterns. In the geochemical classification diagram of Whalen et al. (1987), most of the granites from the Huangshaping and Tuling areas

plot as A-type granites, whereas the Baoshan and Tongshanling granodiorites mainly plot in the I and S-type field (Fig. 9a, b). This classification is further supported by the SiO_2 vs. Zr diagram, in which all the Baoshan and Tongshanling granodiorites plot as I-type granitoids whereas most of the Huangshaping and Tuling granites plot as A-type granites (Fig. 9c). The Baoshan and Tongshanling granodiorites exhibit a negative correlation between SiO_2 and P_2O_5 concentrations, which is characteristic of I-type features (Li et al., 2007a). In contrast, there is no such correlation for the Huangshaping and Tuling granites, indicating they are A-type granites (Fig. 9d).

Although typical I-type granitoids usually have low A/CNK and $\text{K}_2\text{O}/\text{Na}_2\text{O}$ ratios (e.g., Dai et al., 2017), some granodiorite samples from the Baoshan and Tongshanling areas are peraluminous ($\text{A/CNK} > 1.0$) and K-rich ($\text{K}_2\text{O}/\text{Na}_2\text{O} > 1.0$). Peraluminous I-type granitoids may result from crust-mantle interaction (Davis and Hawkesworth, 1993), partial melting of mafic source rocks (Chappell et al., 2012) or fractional crystallization of amphibole (Maulana et al., 2016; Yang

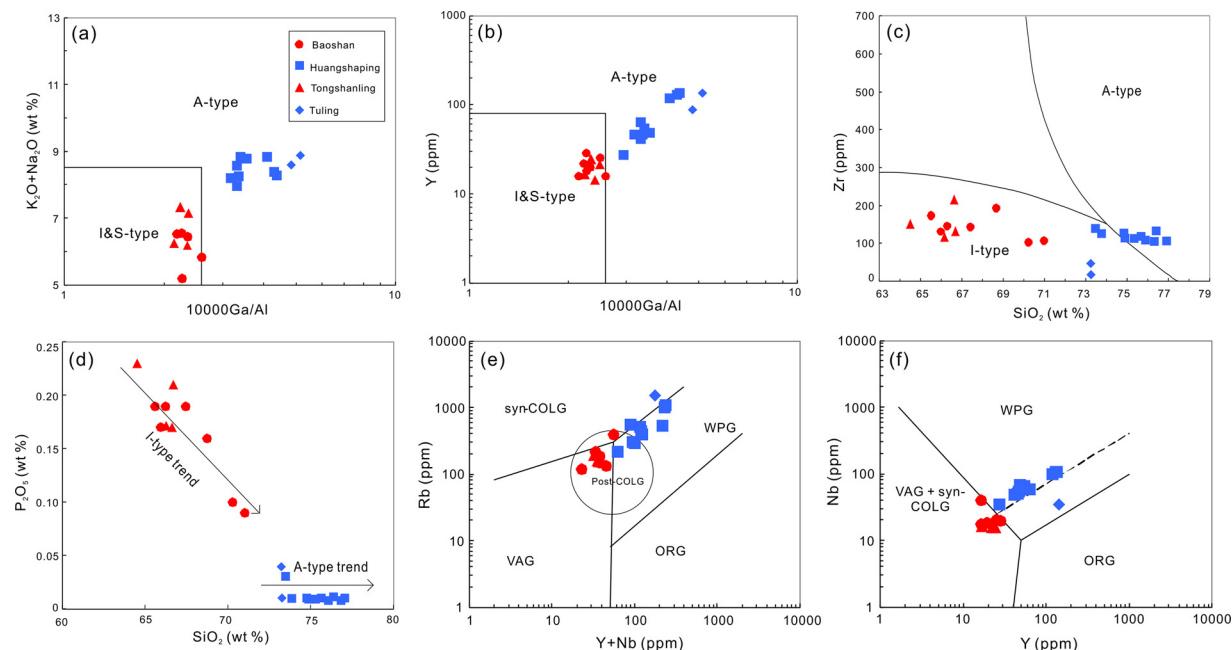


Fig. 9. Geochemical classification for the granitic rocks in South Hunan (after Whalen et al., 1987). (a) 10,000 Ga/Al vs. $K_2O + Na_2O$ (wt %) diagram; (b) 10,000 Ga/Al vs. Nb diagram; (c) SiO_2 vs. Zr diagram; (d) SiO_2 vs. P_2O_5 diagram; (e) Y + Nb vs. Rb diagram and (f) Y vs. Nb diagram. ORG = Ocean Ridge Granites; WPG = Within Plate Granites; VAG = Volcanic Arc Granites; syn-COLG and post-COLG = Syn- and Post-Collision Granites. (a) and (b) after Whalen et al. (1987); (c) after Collins et al. (1982); (e) and (f) after Pearce (1996).

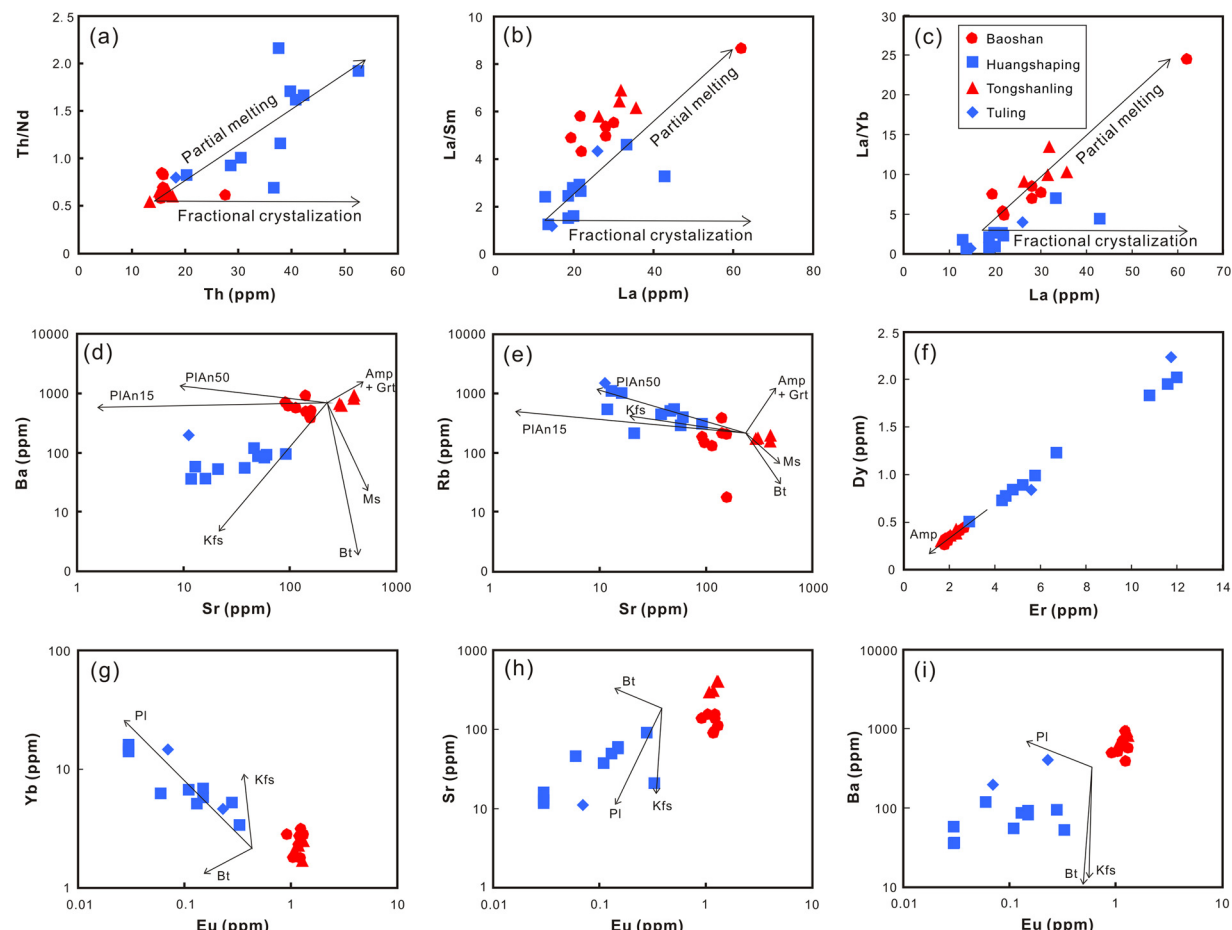


Fig. 10. Magma evolution discrimination diagrams for the granitic rocks in South Hunan. (a) Th vs. Th/Nd; (b) La vs. La/Sm; (c) La vs. La/Yb; (d) Sr vs. Ba; (e) Sr vs. Rb; (f) Er vs. Dy; (g) Eu vs. Yb; (h) Eu vs. Sr; (i) Eu vs. Ba. Trends in (d–i) illustrate crystal fractionation of biotite (Bt), plagioclase (Pl), K-feldspar (Kfs), amphibole (Amp), garnet (Grt) and muscovite (Ms). The partition coefficient data for minerals in equilibrium with granitic liquids are from Rollinson (1993).

et al., 2016). Based on the discrimination plots (Fig. 10a–c), it can be concluded that the parent magma of the granitic rocks from South Hunan was generated by a partial melting process. The parent magmas of the I-type Baoshan and Tongshanling granodiorites underwent limited fractional crystallization of amphibole; however, extensive fractional crystallization took place after initial formation of the magma source for the Huangshaping and Tuling granites, with plagioclase and K-feldspar being important fractionating phases (Fig. 10d–i).

The I-type Baoshan and Tongshanling granodiorites are different from the A-type Huangshaping and Tuling granites not only in granite type and magma evolution but also in tectonic setting. On Rb vs. (Y + Nb) and Nb vs. Y diagrams (Fig. 9e, f), the Baoshan and Tongshanling granodiorites mostly plot as collision-related granites or volcanic arc granites, reflecting a compressional geodynamic environment. In contrast, the Huangshaping and Tuling granites mainly plot in the “within plate granite” field, indicating that they were formed in an extensional setting associated with continental uplift or even tectonic rifting processes.

5.2. Source region of the magmas

The granitoids from the four areas in the southern Hunan Province are basically enriched in large ion lithophile elements (LILE, e.g., Rb, Th, U, K, La) and depleted in Ba, Nb, Sr, P and Ti, indicating they are crust-derived granites (Sun et al., 2017b). However, the variations in major and trace elements and zircon Hf isotopes between these two groups of granitoids suggest a different source region of the magmas. In addition, the formation age of the I- and A-type granites is discontinuous. These features cannot be simply explained by continuous differentiation of a common parental magma (Gu et al., 2017); moreover, it is likely that there is no fractional crystallization relationship between these two kinds of rocks.

Some trace element ratios (e.g., Nb/Ta, Zr/Hf and Th/U) can be used to reveal features of the source rocks of granitic magmas. The Nb/Ta ratios of the I-type Baoshan and Tongshanling granodiorites range from 9.7 to 18 (average = 13, SD = 2.8) and are higher than the average value of Archean continental crust (11, Green, 1995), implying involvement of mantle-sourced materials besides crustal components. In contrast, the A-type Huangshaping and Tuling granites have much lower Nb/Ta ratios (1.6–7.5, averaging 3.7, SD = 2.8) (Table 1), indicating a higher abundance of crustally derived components. The average Zr/Hf ratio of the I-type Baoshan and Tongshanling granodiorites (30) is slightly higher than that of the A-type Huangshaping and Tuling granites (24), but lower than the average value for the mantle (36.5, Taylor and McLennan, 1985). In addition, the average Th/U ratios of the I-type Baoshan and Tongshanling granodiorites (3.6) are higher than the average value for the crust (2.8, Taylor and McLennan, 1985), whereas the A-type Huangshaping and Tuling granites show an opposite trend (average Th/U = 1.8, SD = 0.75). Though Zr/Hf and Th/U ratios in evolved granitic magmas are strongly controlled by accessory mineral fractionation (for Zr/Hf: zircon, for Th/U: allanite, monazite, and to some extent titanite) (Irber, 1999; Zaraisky et al., 2009; Breiter, 2016), the lack of remarkable compositional differences of these accessory minerals between the I-type and A-type granitoids suggest that magmatic sources can be still differentiated by examining these element ratios. All of these indicate that mantle-sourced components have participated in the magmatic processes that generated the I-type granodiorites.

The $\text{Al}_2\text{O}_3/\text{TiO}_2$ and $\text{CaO}/\text{Na}_2\text{O}$ ratios can be applied to determine the lithologic attributes of source rocks and partial melting temperatures of granitic magmas (Sylvester, 1998). As titanium-containing minerals, biotite and ilmenite become unstable under high temperature in the source region, producing increased amounts of Ti in the melts (Clemens and Wall, 1981). Since the $\text{CaO}/\text{Na}_2\text{O}$ ratios are dominantly affected by the plagioclase/clay ratio of the source, granite melts originating from plagioclase-poor, clay-rich sources tend to have lower

$\text{CaO}/\text{Na}_2\text{O}$ ratios (Sylvester, 1998). The I-type Baoshan and Tongshanling granodiorites have low $\text{Al}_2\text{O}_3/\text{TiO}_2$ ratios ranging from 26 to 49 (averaging 35, SD = 6.9) (Table 1), indicating that the partial melting temperature of the source region was higher than 850 °C. In contrast, the $\text{Al}_2\text{O}_3/\text{TiO}_2$ ratios of the A-type Huangshaping and Tuling granites are relatively high (68–670, averaging 323, SD = 239), implying that they are derived from source regions of relatively low melting temperature. Furthermore, the I-type Baoshan and Tongshanling granodiorites tend to have high $\text{CaO}/\text{Na}_2\text{O}$ ratios (averaging 4.3 SD = 5.4), whereas the A-type Huangshaping and Tuling granites mostly have comparatively low values (averaging 1.1, SD = 1.7) (Table 1). Peraluminous granites with high $\text{CaO}/\text{Na}_2\text{O}$ ratios could have been produced through mixing of basaltic melts with pelite-derived melts, but similar ratios cannot be simply explained by anatexis of psammites. All of this indicates that the I-type Baoshan and Tongshanling granodiorites may have been derived from a deep source of basaltic melt mixed with pelite-derived melt. In this setting, crustal anatexis was related to lithospheric delamination and upwelling of hot asthenosphere under high pressures and temperatures.

More information on the contributions to source composition can be obtained by major and trace element discrimination diagrams. In an Rb/Ba vs. Rb/Sr diagram, the I-type Baoshan and Tongshanling granodiorites plot in the clay-poor source region, whereas the A-type Huangshaping and Tuling granites plot in the clay-rich source region (Fig. 11a). The sources can be further distinguished on a molar $\text{Al}_2\text{O}_3/(\text{MgO} + \text{FeO}^\text{T})$ vs. molar $\text{CaO}/(\text{MgO} + \text{FeO}^\text{T})$ diagram, in which the A-type Huangshaping and Tuling granites are revealed to be derived from metapelitic or metagreywacke sources, whereas the I-type Baoshan and Tongshanling granodiorites are interpreted to have formed by the partial melting of metabasaltic to metatonalitic sources (Fig. 11b). In a $\text{CaO}/(\text{FeO}^\text{T} + \text{MgO} + \text{TiO}_2)$ vs. $(\text{CaO} + \text{FeO}^\text{T} + \text{MgO} + \text{TiO}_2)$ diagram, the I-type Baoshan and Tongshanling granodiorites plot along the mixing evolutionary line of argillaceous rock melt and basaltic magma, whereas the A-type Huangshaping and Tuling granites plot in the source region of felsic mudstone and greywacke (Fig. 11c). This indicates that the source rocks of the granodiorites are mainly crustal components but are also mixed with mantle-derived basic materials. Furthermore, in a $(\text{FeO}^\text{T} + \text{MgO} + \text{TiO}_2)$ vs. SiO_2 diagram, the I-type Baoshan and Tongshanling granodiorites mainly plot in the field between biotite gneiss and basalt mixing, whereas the A-type Huangshaping and Tuling granites mostly plot in the clay rocks region (Fig. 11d). All of this further suggests that meta-greywacke could be the source rock of the A-type Huangshaping and Tuling granites.

Due to the stability of zircons, the composition of the Hf isotope system is minimally affected by succeeding geologic events. Thus, Hf isotopes have become an effective method for revealing crustal evolution and tracing the source rocks of magmas. Most $^{176}\text{Lu}/^{177}\text{Hf}$ ratios of zircons in this study are less than 0.002, implying little accumulation of radioactive Hf after zircon crystallization. The calculated initial $^{176}\text{Hf}/^{177}\text{Hf}$ ratios can thus be considered equivalent to the original ratios when the zircons were formed (Wu et al., 2007).

The source region of the granitoids from the four areas in the southern Hunan Province can be divided into two types based on the zircon Hf isotopic features. The A-type Huangshaping and Tuling granites, as well as intrusion I of the Tongshanling porphyritic granodiorite, have very old model ages ($T_{\text{DM1}} = 1454\text{--}2215$ Ma) and crustal model ages ($T_{\text{DM}}^{\text{C}} = 2211\text{--}2974$ Ma), with $\epsilon\text{Hf(t)}$ ratios ranging from -15.84 to -28.31. On a $\epsilon\text{Hf(t)}$ vs. t diagram (Fig. 12), they plot between the 2.5 Ga lower crustal evolution line ($^{176}\text{Lu}/^{177}\text{Hf} = 0.022$) and the 3.0 Ga crustal evolution line ($^{176}\text{Lu}/^{177}\text{Hf} = 0.015$), indicating an ancient crust (Archean-Paleoproterozoic) source region. In contrast, the I-type Baoshan porphyritic granodiorite, granodiorite porphyry and the Tongshanling porphyritic granodiorite (intrusion III) have younger model ages ($T_{\text{DM1}} = 1065\text{--}1302$ Ma) and crustal model ages ($T_{\text{DM}}^{\text{C}} = 1589\text{--}2061$ Ma), with $\epsilon\text{Hf(t)}$ ratios ranging from -5.87 to -11.48. On the $\epsilon\text{Hf(t)}$ vs. t diagram (Fig. 12), they plot above the 2.5 Ga lower

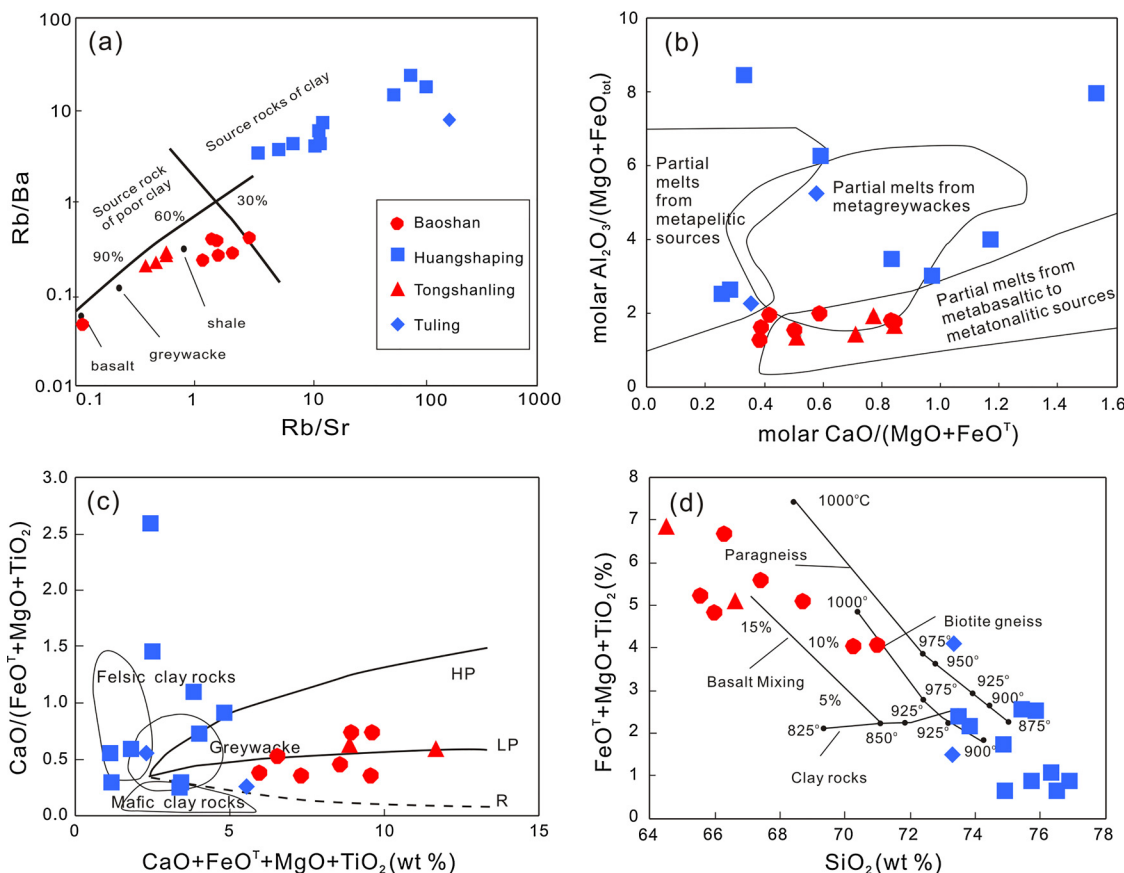


Fig. 11. Source region discrimination diagrams for granitic rocks from South Hunan. (a) Rb/Ba vs. Rb/Sr diagram (after Sylvester, 1998); (b) molar $\text{Al}_2\text{O}_3/(\text{MgO} + \text{FeOT})$ vs. molar $\text{CaO}/(\text{MgO} + \text{FeOT})$ diagram (after Altherr et al., 2000); (c) $\text{CaO}/(\text{FeOT} + \text{MgO} + \text{TiO}_2)$ vs. $(\text{CaO} + \text{FeOT} + \text{MgO} + \text{TiO}_2)$ (wt %) diagram (after Patiño Douce, 1999); HP and LP thick solid lines are reaction curves for high and low pressure that model the melt compositions that are produced by hybridization of high-Al olivine tholeiite with metagreywacke. The R dash-dot lines are reaction curves for low pressure hybridization of calc-alkaline granites with high-Al olivine tholeiites, with production of plagioclase + orthopyroxene. (d) $(\text{FeOT} + \text{MgO} + \text{TiO}_2)$ vs. SiO_2 diagram (after Sylvester, 1998).

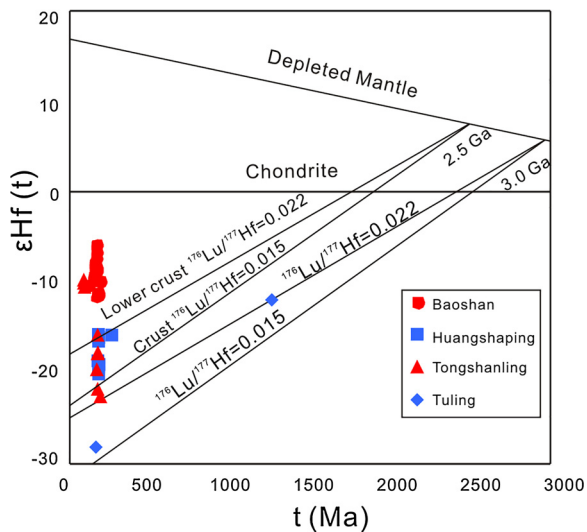


Fig. 12. Zircon $\epsilon\text{Hf}(t)$ vs. t diagrams for the granitic rocks from South Hunan.

crustal evolution line ($^{176}\text{Lu}/^{177}\text{Hf} = 0.022$, $f_{\text{Lu/Hf}} = -0.34$), implying that the source rock region is ancient lower crust with input of mantle-derived components. All of this may indicate that the magma source region of the Tongshanling-Tuling plutons is generally deeper than that of the Baoshan-Huangshaping plutons.

In addition, large variations of $\epsilon\text{Hf}(t)$ values occur in intrusion I from the Tongshanling area. Zircon Hf isotopic ratios are invariant with

partial melting or fractional crystallization. Thus, the large variations of $\epsilon\text{Hf}(t)$ values indicate that the Hf isotopic composition in the source region is heterogeneous. This heterogeneity can be interpreted as the effect of interaction between two end-member sources: more radioactive Hf in the mantle and less radioactive Hf in the crust (Griffin et al., 2002; Bolhar et al., 2008). Consequently, the large variations of $\epsilon\text{Hf}(t)$ values in intrusion I from the Tongshanling area can be ascribed to the mixing of mantle-derived and crust-derived magmas. The juvenile mantle-derived magma induced melting of ancient crustal materials and mixed with the crust-derived melts, forming intrusion I.

A magmatic source region formed in an early extensional setting usually has mantle-derived juvenile crustal components (Rutanen et al., 2011; Chen et al., 2008). The I-type Baoshan and Tongshanling granodiorites were formed in such a tectonic setting, reflecting a transitional environment from compression to extension. The compositions of these metaluminous to peraluminous high-K calc-alkaline I-type granitoids could result from mixing of magmas derived from mantle and crustal components (Karsli et al., 2010; Aydin, 2014). Recent studies reported the occurrence of dark mafic enclaves in the granodiorites, suggesting partial melting of crustal components that could be related to the underplating of mantle-derived magma (Xie et al., 2013). Heating from the asthenosphere subsequently resulted in intensive magmatism. In contrast, the A-type Huangshaping and Tuling granites were derived from crust in a well-developed extensional setting that had little interaction with mantle-sourced components.

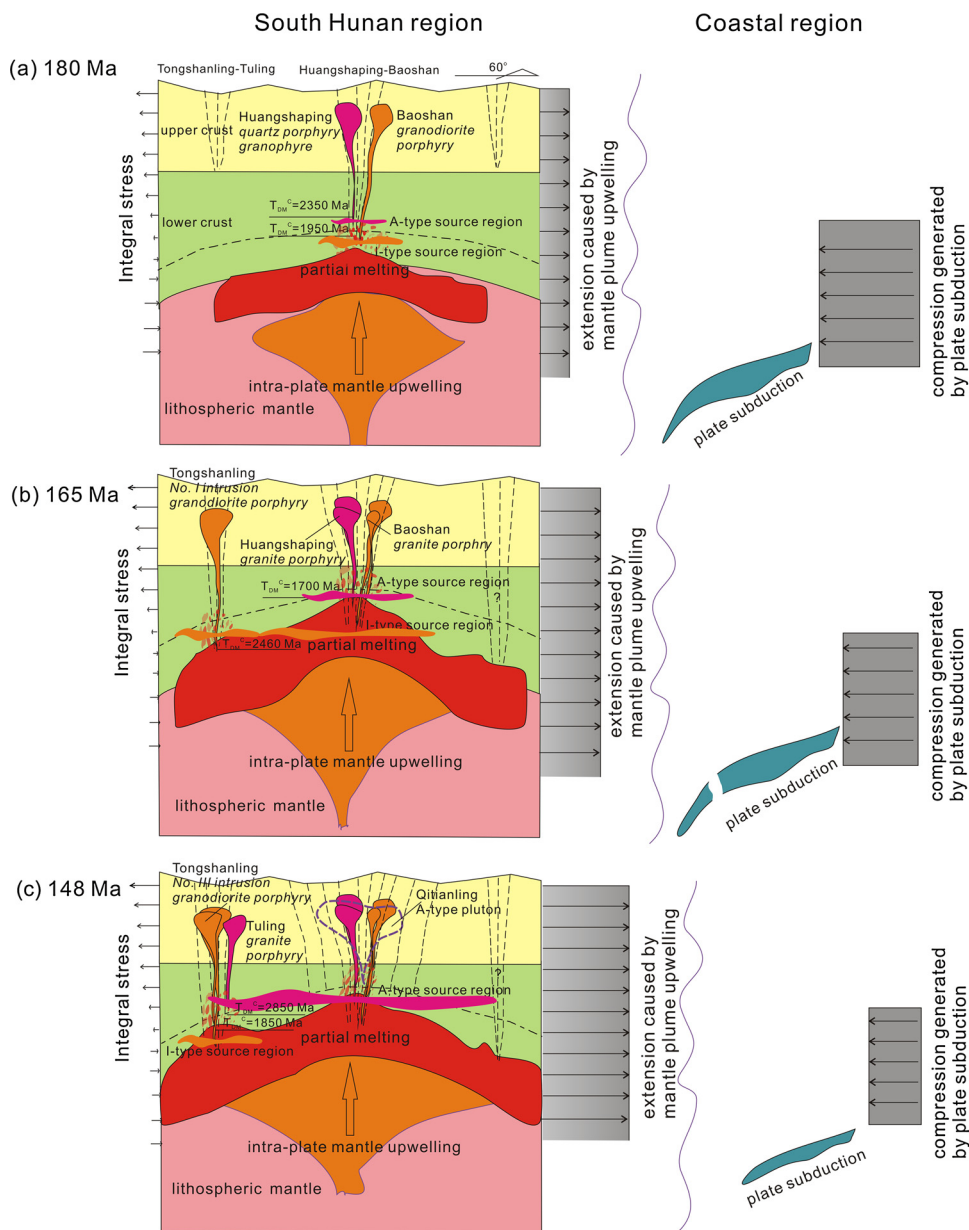


Fig. 13. Block diagram illustrating the genesis of the spatially and temporally associated I- and A-type granites in South Hunan.

5.3. Co-development model for the I- and A-type granites

Spatially and temporally associated I- and A-type granites are not unique to South Hunan. They have been occasionally reported throughout the world, such as in the western margin of the Yangtze Block (Zhao et al., 2008), the South Tien Shan suture (Konopelko et al., 2009), the Pataz gold-mining district in northern Peru (Witt et al., 2014), the North Eastern Desert in Egypt (El-Bialy and Omar, 2015), the eastern Jiamusi Massif, NE China (Bi et al., 2016), the Sanandaj-Sirjan Zone, NW Iran (Sarjoughian et al., 2016), and the Eastern Pontides, NE Turkey (Karsli et al., 2010, 2012; Aydin, 2014). Different models have been proposed to explain the genesis of these spatially and temporally associated I- and A-type granites, and most of the models take into account the co-development of different source regions and distinct temperature-pressure environments. At the western margin of the Yangtze Block, the A-type magma source region was situated above that of I-type, and aluminous A-type granite was generated by large-scale magmatic underplating (Zhao et al., 2008). The contemporaneous post-collisional barren I-type versus tin-bearing A-type granites on opposite

sides of the South Tien Shan suture have also been ascribed to dichotomous sources (Konopelko et al., 2009). In the Pataz gold-mining district, mantle-derived magmas in andesitic lower crust caused partial melting and generated calc-alkaline (I-type) granitoids, whereas relatively K-rich (A-type) magmas were formed by melting of a mid-crustal tonalitic source (Witt et al., 2014). Differences in magma source also occur in the Arabian-Nubian Shield, where the earlier intruded I-type granite evolved through assimilation and fractional crystallization processes from mantle-derived parental magmas, whereas the A-type granite was derived from a high degree of partial melting of metasedimentary sources (El-Bialy and Omar, 2015). In the eastern Jiamusi Massif (NE China), the aluminous A-type granite magmas were probably derived by high-temperature partial melting of a felsic crustal source, whereas the I-type granite magmas probably resulted from partial melting of a mafic lower crust (Bi et al., 2016). Sarjoughian et al. (2016) proposed that the geochemical differences among the I- and A-type rock suites in the Sanandaj-Sirjan Zone are likely to indicate different melt origins. The transition from I-type to A-type magmatism may have resulted from a change in the geodynamic regime from

compression to extension. According to Karsli et al (2018), the late Cretaceous A- and I-type magmas in the Eastern Pontides region were derived from a similar source material at different P-T conditions. The A-type magmatic activity was particularly related to the final stage of slab roll-back of the Neo-Tethyan oceanic lithosphere, which correlates to the end of the subduction. Though these models can explain the co-development of I- and A-type granites in some specific area, none of them can be adopted to interpret the case in South Hunan. Thus, a new model is needed not only to explain the spatially and temporally associated I- and A-type granites in South Hunan but also to provide insights into the co-development of different types granites in the world.

Based on the major and trace element and Hf isotope studies on the granitoids from South Hunan, two pairs of I- and A-type plutons have been identified in this study. The co-development of the I- and A-type plutons may reflect different depths of the source region, i.e., shallower for the A-type and deeper for the I-type (Jiang et al., 2011; Machowiak and Stawikowski, 2012). In addition, the geochemical differences may also indicate distinct tectonic environments: extension for the A-type and compression for the I-type (Yan and Shi, 2016; Sarjoughian et al., 2016). All of this reveals a vertical zoning of the source region and dynamic stress environment for the generation of the I- and A-type magmas in South Hunan.

Previous research pointed out that the development of the South Hunan region of South China was governed by a combined tectonic framework of intra-plate mantle uplift and paleo-Pacific plate subduction (Quan et al., 2013b; Jiang et al., 2015; Guo et al., 2015). The crustal thinning and mantle uplifting during the Jurassic were the effects of a combination of intra-plate mantle activity and subduction of the paleo-Pacific plate (Mao et al., 2014; Li et al., 2016c). The zone of initiation of mantle upwelling is estimated to be close to the Baoshan-Huangshaping area and beneath the Qitianling-Jiuyishan granitic plutons, where many dark mafic enclaves have been observed and intense mantle-crust interactions have been identified (Zhu et al., 2009; Zhao et al., 2012). The trigger and mechanism of the mantle upwelling can be ascribed to the combined effects of the paleo-Pacific plate subduction (Mao et al., 2007) and the intraplate mantle uplift (Zhang et al., 2009; Quan et al., 2013b) as described in more detail below.

This study proposes a new model to explain the genesis of the spatially and temporally associated I- and A-type granites in South Hunan (Fig. 13). The differences in stress and temperature owing to partial melting, varied compositions of the source regions, and different tectonic environments are the major factors controlling the co-development of the I- and A-type granites. Mantle upwelling led to a stable extension force in the crust, whereas plate subduction mainly resulted in lateral extrusion pressure in particular sections. Compressive stress caused by plate subduction is maximum at depth and gradually decreased nearer to the surface (Ellis, 1996). In contrast, extensional stress resulting from mantle upwelling appears to have no correlation with depth (Henk, 2006; Komut et al., 2012). Consequently, the resulting scenario for the tectonic development of South Hunan is that extrusion pressure mostly occurred in the deep crust while increased extensional stress dominated the shallower portions. Crustal extension can be driven by mantle upwelling (Faccenna et al., 2008; Li et al., 2018b; Sun et al., 2018, in press). Thus, the A-type granites in South Hunan may have formed in an extensional environment caused by mantle upwelling, whereas the I-type granitoids could have formed in a compressional setting caused by plate subduction. Moreover, the crustal source regions are not homogeneous. This has been revealed in this study by major and trace element compositions as well as zircon Hf isotope analysis. The different structural layers combined with the variability of the source regions produced the associations of I- and A-type granites in the study area. Consequently, the detailed formation process of the I- and A-type granite pairs in South Hunan can be summarized as follows:

At ~180 Ma, mantle upwelling was activated by the generation of a deep-sourced intra-plate mantle upwelling, coupled with the

subduction of the paleo-Pacific plate. Partial melting of the source region in the lower crust was triggered by mantle underplating (Yu et al., 2003). Ancient mantle lithosphere thinned and was replaced by hotter, younger mantle, leading to abundant magmatism (Liu et al., 2012). This formed high temperature I-type magma under compressive stress in the deeper portions while A-type magma was generated under extensional stress in the shallower parts of the crust. The source region at depth consisted mainly of basic components derived from juvenile ingredients in the asthenospheric mantle, with an average crustal model age of ~1950 Ma. This intense mantle-crust interaction has been recorded by mafic enclaves in the I-type Baoshan porphyritic granodiorite (Xie et al., 2013). The composition of the source region in the shallower portion is equivalent to assorted sandstone and is less affected by mantle-crust interaction, with a much older average crustal model age of ~2350 Ma. Meanwhile, early-middle Jurassic mafic magmas were also generated to form the Changchengling and Ningyuan basaltic rocks (178–170 Ma) in southern Hunan, which show active continental features with OIB-like element and isotopic compositions (Jiang et al., 2009; Wang et al., 2013). This indicates that oceanic crust was subducted into the asthenospheric mantle. Lithospheric thinning, delamination and rifting developed progressively from the surface to the deeper portions, and rift-associated fractures reached the zone of mantle upwelling, becoming the channels for the ascending magmas (Fig. 13a). Regionally, these magmas developed in response to a post-orogenic stage dextral strike-slip system which was initiated by far-field oblique stresses from the incipient subduction of the paleo-Pacific oceanic plate (Shu et al., 2009; Cai, 2013).

By 165 Ma, the mantle upwelling continued to increase with the rise of the deep-sourced mantle and breakup of the subducted paleo-Pacific plate. This led to reinforced extensional stress in the shallower part and weakened extrusion pressure from the deeper portions. Under these conditions, magmas of the I-type Baoshan granodiorite porphyry and A-type Huangshaping granite porphyry were successively generated from different source regions at different temperatures. The I- and A-type magma source regions were moderately shallower than the previous source during ~180 Ma, with average crustal model ages of ~1700 Ma and ~1550 Ma, respectively. These magmas intruded along the more evolved channels above the mantle upwelling center, forming the later phases of the Baoshan and Huangshaping plutons. At the same time, the partial melting region expanded laterally and the vertical channels on both sides continued to develop towards the deeper portions. They met at the source region of the Tongshanlong porphyritic granodiorite (intrusion I), forming an I-type magma under a compressional environment. Compared to the Baoshan I-type magmas, the I-type magma from the Tongshanlong area received less crust-mantle interaction due to the greater distance from the mantle upwelling front belt. Thus the source region has an older, less disturbed average crustal model age of 2460 Ma (Fig. 13b). The generation of these magmas was a response to the initial stage of tectonic rifting (Shu et al., 2009).

At 165–148 Ma, the continued mantle upwelling was mainly driven by the lateral expansion of the uplifted mantle and less so by the subducted plate. Greater amounts of mantle components were added into the crust to become important magma sources. The partial melting region underwent a vertical and lateral expansion under an extensional regime, resulting in a major period for emplacement of the A-type granites and related mineral resources in the Qitianling area. The widely distributed A-type granites imply a peak period of intracontinental extension (Shu et al., 2009; Xu et al., 2016). Anatexis in the middle crust was promoted by a second batch of magma derived from the undepleted metasomatised asthenosphere. On the other hand, the extensional channels in the outer zones of the pluton (beneath the Tongshanlong and Tuling areas) continued to develop, successively forming the I-type and A-type magmas from distinct source regions under a transitional stress environment (from compression to extension). The I-type magma source region of the Tongshanlong porphyritic granodiorite (intrusion III) received more juvenile components from the

mantle compared to the A-type magma source region of the Tuling granite porphyry, with average crustal model ages of ~1850 Ma and ~2850 Ma, respectively (Fig. 13c). During this stage, the late Jurassic Daoxian and Guiyang mafic rocks (152–146 Ma) were derived directly from partial melting of shallower (60–100 km) lithospheric mantle, which shows shoshonitic affinities that are compatible with a continental arc-rifting setting (Jiang et al., 2009).

6. Conclusion

- Two pairs of spatially and temporally associated I- and A-type granites have been identified in the southern Hunan Province, South China. The Baoshan and Tongshanling I-type plutons have zircon LA-ICPMS ages ranging from 180 to 148 Ma, and the Huangshaping and Tuling A-type granites have ages ranging from 180 to 158 Ma.
- Compared to the I-type granodiorites, the A-type granites have higher concentrations of SiO₂ but lower TiO₂, Al₂O₃, total FeO, MgO and P₂O₅ contents. They are more enriched in Rb, Th, U, Ga, Hf and HREE and significantly depleted in Ba, Sr and Eu. The I-type granodiorites plot as collision-related granites formed in a compressional environment, whereas the A-type granites are classified as within-plate granites generated in an extensional setting.
- The I-type granodiorites may have been derived from a deep source of basaltic melts mixed with pelite-derived melts, whereas metagreywacke could be the source rock for the A-type granites. Zircon Hf isotope analysis suggests that the source region for the I-type magmas was influenced by mantle-derived juvenile crustal components. In contrast, the A-type granites were derived from ancient crust with little interaction from mantle-sourced components.
- A new model is proposed to explain the genesis of the spatially and temporally associated I- and A-type granites in South Hunan. The pressure and temperature differences in source regions caused by combined effects of intra-plate mantle upwelling and paleo-Pacific plate subduction are the major controlling factors of the jointly developed formation of the two types of granites. Crustal anatexis was associated with lithospheric delamination and upwelling of hot asthenosphere under high pressure and temperature, forming the I-type magmas. The A-type magmas were formed in the shallower portions of the crust where extensional stress was dominant and mantle-crust interaction was weak.

Acknowledgements

This work was co-financed by the National Key Research and Development Plan (Grant No. 2018YFC0603902), the Special Survey for Mineral Resources Evaluation from the China Geological Survey (Grant Nos. 1212011121116 & 1212011085372) and the National Natural Science Foundation of China (Grant No. 41502067). We thank Guoxiang Chi for his constructive comments on an earlier version of the manuscript. We are grateful to Astrid Holzheid (Editor-in-Chief), Axel Schmitt and Faruk Aydin for constructive suggestions and criticisms in reviewing the manuscript.

References

- Ai, H., 2013. Zircon U–Pb geochronology and Hf isotopic compositions of ore-related granites from Huangshaping polymetallic deposit of Hunan Province. *Miner. Deposits* 32, 545–563 (in Chinese with English abstract).
- Altherr, R., Holl, A., Hegner, E., Langer, C., Kreuzer, H., 2000. High-potassium, calc-alkaline I-type plutonism in the European Variscides: Northern Vosges (France) and Northern Schwarzwald (Germany). *Lithos* 50, 51–73.
- Aydin, F., 2014. Geochronology, geochemistry, and petrogenesis of the Macka sub-volcanic intrusions: implications for the Late Cretaceous magmatic and geodynamic evolution of the eastern part of the Sakarya Zone, northeastern Turkey. *Int. Geol. Rev.* 56, 1246–1275.
- Bai, D.Y., Zhou, L., Wang, X.H., Zhang, X.Y., Ma, T.Q., 2007. Tectonic-magmatic mechanisms of the two types of early Yanshanian W-Sn-polyetalllic and Pb-Zn-polymetallic deposit assemblages in southeast Hunan. *Acta Geol. Sin.* 81, 1238–1247 (in Chinese with English abstract).
- Bi, J.H., Ge, W.C., Yang, H., Wang, Z.H., Xu, W.L., Yang, J.H., Xing, D.H., Chen, H.J., 2016. Geochronology and geochemistry of late Carboniferous-middle Permian I- and A-type granites and gabbro-diorites in the eastern Jiamusi Massif, NE China: implications for petrogenesis and tectonic setting. *Lithos* 266–267, 213–232.
- Blichert-Toft, J., Albarède, F., 1997. The Lu–Hf isotope geochemistry of chondrites and the evolution of the mantle–crust system. *Earth Planet. Sci. Lett.* 148, 243–258.
- Bolhar, R., Weaver, S.D., Whitehouse, M.J., Palin, J.M., Woodhead, J.D., Cole, J.W., 2008. Sources and evolution of arc magmas inferred from coupled O and Hf isotope systematics of plutonic zircons from the Cretaceous Separation Point Suite (New Zealand). *Earth Planet. Sci. Lett.* 268, 312–324.
- Breiter, K., 2016. Monazite and zircon as major carriers of Th, U, and Y in peraluminous granites: examples from the Bohemian Massif. *Mineral. Petrol.* 110, 767–785.
- Cai, J.X., 2013. An early Jurassic dextral strike-slip system in southern South China and its tectonic significance. *J. Geodyn.* 63, 27–44.
- Cao, J., Wu, Q., Yang, X., Kong, H., Li, H., Xi, Huang, Q., Liu, B., 2018a. Geochronology and genesis of the Xitian W-Sn polymetallic deposit in eastern Hunan Province, South China: evidence from zircon U-Pb and muscovite Ar-Ar dating, petrochemistry, and wolframite Sr-Nd-Pb isotopes. *Minerals*. <https://doi.org/10.3390/min8030111>.
- Cao, J., Yang, X., Du, J., Wu, Q., Kong, H., Li, H., Wan, Q., Xi, X., Gong, Y., Zhao, H., 2018b. Formation and geodynamic implication of the Early Yanshanian granites associated with W-Sn mineralization in the Nanling range, South China: an overview. *Int. Geol. Rev.* <https://doi.org/10.1080/00206814.2018.1466370>. in press.
- Cen, T., Li, W.X., Wang, X.C., Pang, C.J., Li, Z.X., Xing, G.F., Zhao, X.L., Tao, J.H., 2016. Petrogenesis of early Jurassic basalts in southern Jiangxi Province, South China: implications for the thermal state of the Mesozoic mantle beneath South China. *Lithos* 256–257, 311–330.
- Chappell, B.W., Bryant, C.J., Wyborn, D., 2012. Peraluminous I-type granites. *Lithos* 153, 142–153.
- Charvet, J., 2013. The Neoproterozoic–early Paleozoic tectonic evolution of the South China block: an overview. *J. Asian Earth Sci.* 74, 198–209.
- Chen, J.F., Jahn, B.M., 1998. Crustal evolution of southeastern China: Nd and Sr isotopic evidence. *Tectonophysics* 284, 101–133.
- Chen, P.R., Hua, R.M., Zhang, B.T., Lu, J.J., Fan, C.F., 2002. Early Yanshanian post-orogenic granitoids in the Nanling region—petrological constraints and geodynamic settings. *Sci. China Ser. D Earth Sci.* 45, 755–768.
- Chen, B., Tian, W., Jahn, B.M., Chen, Z.C., 2008. ZirconSHRIMP U–Pb ages and in-situ Hf isotopic analysis for the Mesozoic intrusions in South Taihang, North China craton: evidence for hybridization between mantle-derived magmas and crustal components. *Lithos* 102, 118–137.
- Chen, Y.X., Li, H., Sun, W.D., Ireland, T., Tian, X.F., Hu, Y.B., Yang, W.B., Chen, C., Xu, D.R., 2016. Generation of late mesozoic qianlishan A2-type granite in Nanling Range, South China: implications for shizhuayan W-Sn mineralization and tectonic evolution. *Lithos* 266–267, 435–452.
- Clemens, J.D., Wall, V.J., 1981. Origin and crystallization of some peraluminous (S-type) granitic magmas. *Can. Mineral.* 19, 111–131.
- Collins, W., Beams, S., White, A., Chappell, B., 1982. Nature and origin of A-type granites with particular reference to southeastern Australia. *Contrib. Mineral. Petrol.* 80, 189–200.
- Dai, Y.P., Zhu, Y.D., Li, T.Z., Zhang, H.H., Tang, G.L., Shen, Z.W., 2017. A crustal source for ca. 165 Ma post-collisional granites related to mineralization in the Jianglang dome of the Songpan-Ganzi Orogen, eastern Tibetan Plateau. *Chemie Der Erde Geochem.* 77, 573–586.
- Davis, J., Hawkesworth, C., 1993. The petrogenesis of 30–20 Ma basic and intermediate volcanics from the Mogollon-Datil Volcanic Field, New Mexico, USA. *Contrib. Mineral. Petrol.* 115, 165–183.
- Deng, Z., Liu, S., Zhang, L., Wang, Z., Wang, W., Yang, P., Luo, P., Guo, B., 2014. Geochronology, zircon U–Pb and Lu–Hf isotopes of an Early Cretaceous intrusive suite in northeastern Jiangxi Province, South China Block: implications for petrogenesis, crust/mantle interactions and geodynamic processes. *Lithos* 200–201, 334–354.
- Diwu, C.R., Sun, Y., Zhang, H., Wang, Q., Guo, A.L., Fan, L.G., 2012. Episodic tectono-thermal events of the western North China Craton and North Qinling Orogenic Belt in central China: constraints from detrital zircon U–Pb ages. *J. Asian Earth Sci.* 47, 107–122.
- El-Bialy, M.Z., Omar, M.M., 2015. Spatial association of Neoproterozoic continental arc I-type and post-collision A-type granitoids in the Arabian–Nubian Shield: The Wadi Al-Baroud Older and Younger Granites North Eastern Desert, Egypt. *J. Afr. Earth Sci.* 103, 1–29.
- Ellis, S., 1996. Forces driving continental collision: reconciling indentation and mantle subduction tectonics. *Geology* 24, 699–702.
- Faccenna, C., Rossetti, F., Becker, T.W., Danesi, S., Morelli, A., 2008. Recent extension driven by mantle upwelling beneath the Admiralty Mountains (East Antarctica). *Tectonics* 27. <https://doi.org/10.1029/2007TC002197>.
- Frost, B.R., Barnes, C.G., Collins, W.J., Arculus, R.J., Ellis, D.J., Frost, C.D., 2001. A geochemical classification for granitic rocks. *J. Petrol.* 42, 2033–2048.
- Geological Survey of South Hunan (GSSH), 2008. The Instructions of 1:50,000 Regional Geological Survey on the Gongwu Region (in Chinese). pp. 1–18.
- Green, T.H., 1995. Significance of Nb/Ta as an indicator of geochemical process in the crust–mantle system. *Chem. Geol.* 120, 347–359.
- Griffin, W.L., Pearson, N.J., Belousova, E., Jackson, S.E., van Achterbergh, E., O'Reilly, S.Y., Shee, S.R., 2000. The Hf isotope composition of cratonic mantle: LAM-MC-ICPMS analysis of zircon megacrysts in kimberlites. *Geochim. Cosmochim. Acta* 64, 133–147.
- Griffin, W.L., Wang, X., Jackson, S.E., Pearson, N.J., O'Reilly, S.Y., Xu, X., Zhou, X., 2002. Zircon chemistry and magma mixing, SE China: in-situ analysis of Hf isotopes, Tonglu and Pingtan igneous complexes. *Lithos* 61, 237–269.
- Gu, H., Yang, X., Deng, J., Duan, L., Liu, L., 2017. Geochemical and zircon U–Pb

- geochronological study of the Yangshan A-type granite: insights into the geological evolution in south Anhui, eastern Jiangnan Orogen. *Lithos* 284–285, 156–170.
- Guo, C.L., Wang, R.C., Yuan, S.D., Wu, S.H., Yin, B., 2015. Geochronological and geochemical constraints on the petrogenesis and geodynamic setting of the Qianlishan granitic pluton, Southeast China. *Mineral. Petrol.* 109, 253–282.
- He, Z.Y., Xu, X.S., Niu, Y.L., 2010. Petrogenesis and tectonic significance of a Mesozoic granite–syenite–gabbro association from inland South China. *Lithos* 119, 621–641.
- Henk, A., 2006. Stress and strain during fault-controlled lithospheric extension—insights from numerical experiments. *Tectonophysics* 415, 39–55.
- Hoskin, P.W.O., Schaltegger, U., 2003. The composition of zircon and igneous and metamorphic petrogenesis. In: In: Hanchar, J.M., Hoskin, P.W.O. (Eds.), *Zircon: Reviews in Mineralogy and Geochemistry* Vol. 53. pp. 27–62.
- Hsieh, P.S., Chen, C.H., Yang, H.J., Lee, C.Y., 2008. Petrogenesis of the Nanling Mountains granites from South China: constraints from systematic apatite geochemistry and whole-rock geochemical and Sr–Nd isotope compositions. *J. Asian Earth Sci.* 33, 428–451.
- Hsu, K.J., Li, J.I., Chen, H.H., Wang, Q.C., Sun, S., Sengor, A.M.C., 1990. Tectonics of south China—key to understanding West Pacific geology. *Tectonophysics* 183, 9–39.
- Hu, R.Z., Wei, W.F., Bi, X.W., Peng, J.T., Qi, Y.Q., Wu, L.Y., Chen, Y.W., 2012. Molybdenite Re–Os and muscovite $^{40}\text{Ar}/^{39}\text{Ar}$ dating of the Xihuashan tungsten deposit, central Nanling district, South China. *Lithos* 150, 111–118.
- Hua, R.M., Zhang, W.L., Chen, P.R., Wang, R.C., 2003. Comparison in the characteristics, origin, and related metallogeny between granites in Dajishan and Piaotang, Southern Jiangxi, China. *Geol. J. China Univ.* 9, 609–619 (in Chinese with English abstract).
- Hua, R.M., Zhang, W.L., Gu, S.Y., Chen, P.R., 2007. Comparison between REE granite and W–Sn granite in the Nanling region, South China, and their mineralization. *Acta Petrol. Sin.* 23, 2321–2328 (in Chinese with English abstract).
- Huang, X.D., Lu, J.J., Sizaret, S., Wang, R.C., Ma, D.S., Zhang, R.Q., Zhao, X., Wu, J.W., 2017. Petrogenetic differences between the Middle-Late Jurassic Cu–Pb–Zn-bearing and W-bearing granites in the Nanling Range, South China: a case study of the Tongshanling and Weijia deposits in southern Hunan Province. *Sci. China-Earth Sci.* 60, 1220–1236.
- Irber, W., 1999. The lanthanide tetrad effect and its correlation with K/Rb, Eu/Eu*, Sr/Eu, Y/Ho, and Zr/Hf of evolving peraluminous granite suites. *Geochim. Cosmochim. Acta* 63, 489–508.
- Jiang, Y.H., Jiang, S.Y., Dai, B.Z., Liao, S.Y., Zhao, K.D., Ling, H.F., 2009. Middle to late Jurassic felsic and mafic magmatism in southern Hunan province, southeast China: implications for a continental arc to rifting. *Lithos* 107, 185–204.
- Jiang, Y.H., Zhao, P., Zhou, Q., Liao, S.Y., Jin, G.D., 2011. Petrogenesis and tectonic implications of Early Cretaceous S- and A-type granites in the northwest of the Gan-Hang rift, SE China. *Lithos* 121, 55–73.
- Jiang, Y.H., Wang, G.C., Liu, Z., Ni, C.Y., Qing, L., Zhang, Q., 2015. Repeated slab advance-retreat of the Palaeo-Pacific plate underneath SE China. *Int. Geol. Rev.* 57, 472–491.
- Jiang, W.C., Li, H., Wu, J.H., Zhou, Z.K., Kong, H., Cao, J.Y., 2018a. A newly found biotite syenogranite in the Huangshaping polymetallic deposit, South China: insights into Cu mineralization. *J. Earth Sci.* 29, 537–555.
- Jiang, W., Li, H., Evans, N.J., Wu, J., Cao, J., 2018b. Metal sources of world-class polymetallic W–Sn skarns in the Nanling Range, South China: Granites versus sedimentary rocks? *Minerals*. <https://doi.org/10.3390/min8070265>.
- Karsli, O., Dokuz, A., Uysal, I., Aydin, F., Chen, B., Kandemir, R., Wijbrans, J., 2010. Relative contributions of crust and mantle to generation of Campanian high-K calc-alkaline I-type granitoids in a subduction setting, with special reference to the Hartsit Pluton, Eastern Turkey. *Contrib. Mineral. Petrol.* 160, 467–487.
- Karsli, O., Caran, S., Dokuz, A., Coban, H., Chen, B., Kandemir, R., 2012. A-type granitoids from the Eastern Pontides, NE Turkey: records for generation of hybrid A-type rocks in a subduction-related environment. *Tectonophysics* 530, 208–224.
- Karsli, O., Aydin, F., Uysal, I., Dokuz, A., Kumral, M., Kandemir, R., Budakoglu, M., Ketenci, M., 2018. Latest Cretaceous “A2-type” granites in the Sakarya Zone, NE Turkey: partial melting of mafic lower crust in response to roll-back of Neo-Tethyan oceanic lithosphere. *Lithos* 302–303, 312–328.
- Komut, T., Gray, R., Pysklywec, R., Göğüş, O.H., 2012. Mantle flow uplift of western Anatolia and the Aegean: interpretations from geophysical analyses and geodynamic modeling. *J. Geophys. Res.* 117, B11412. <https://doi.org/10.1029/2012JB009306>.
- Konopelko, D., Seltmann, R., Biske, G., Lepekina, E., Sergeev, S., 2009. Possible source dichotomy of contemporaneous post-collisional barren I-type versus tin-bearing A-type granites, lying on opposite sides of the South Tien Shan suture. *Ore Geol. Rev.* 35, 206–216.
- Le Bas, M.J., Le Maitre, R.W., Streckeisen, A., Zanettin, B., 1986. A chemical classification of volcanic rocks based on the total alkali–silica diagram. *J. Petrol.* 27, 745–750.
- Le Maitre, R.W., 1989. A Classification of Igneous Rocks and Glossary of Terms: Recommendations of the IUGS Commission on the Systematics of Igneous Rocks. Blackwell, Oxford, pp. 1–34.
- Li, Z.X., Li, X.H., 2007. Formation of the 1300-km-wide intracontinental orogen and postorogenic magmatic province in Mesozoic South China: a flat-slab subduction model. *Geology* 35, 179–182.
- Li, X.H., Chung, S.L., Zhou, H.W., Lo, C.H., Liu, Y., Chen, C.H., 2004. Jurassic intraplate magmatism in southern Hunan-eastern Guangxi: $^{40}\text{Ar}/^{39}\text{Ar}$ dating, geochemistry, Sr–Nd isotopes and implications for tectonic evolution of SE China. In: In: Malpas, J., Fletcher, C.J., Aitchison, J.C., Ali, J. (Eds.), *Aspects of the Tectonic Evolution of China* Vol. 226. Geological Society Special Publication, pp. 193–216.
- Li, X.H., Li, W.X., Li, Z.X., 2007a. On the genetic classification and tectonic implications of the Early Yanshanian granitoids in the Nanling Range, South China. *Chin. Sci. Bull.* 52, 1873–1885.
- Li, X.H., Li, Z.X., Li, W.X., Liu, Y., Yuan, C., Wei, G.J., Qi, C.S., 2007b. U–Pb zircon, geochemical and Sr–Nd–Hf isotopic constraints on age and origin of Jurassic I- and A-type granites from central Guangdong, SE China: a major igneous event in response to foondering of a subducted flat-slab? *Lithos* 96 (1–2), 186–204.
- Li, X.H., Li, W.X., Wang, X.C., Li, Q.L., Liu, Y., Tang, G.Q., 2009. Role of mantle-derived magma in genesis of early Yanshanian granites in the Nanling Range, South China: in situ zircon Hf–O isotopic constraints. *Sci. China Ser. D Earth Sci.* 52, 1262–1278.
- Li, Z.X., Li, X.H., Wartho, J.A., Clark, C., Li, W.X., Zhang, C.L., Bao, C., 2010. Magmatic and metamorphic events during the early Paleozoic Wuyi-Yunkai orogeny, south-eastern South China: new age constraints and pressure-temperature conditions. *Geol. Soc. Am. Bull.* 122, 772–793.
- Li, H., Watanabe, K., Yonezu, K., 2014a. Zircon morphology, geochronology and trace element geochemistry of the granites from the Huangshaping polymetallic deposit, South China: implications for the magmatic evolution and mineralization processes. *Ore Geol. Rev.* 60, 14–35.
- Li, H., Watanabe, K., Yonezu, K., 2014b. Geochemistry of A-type granites in the Huangshaping polymetallic deposit (South Hunan, China): implications for granite evolution and associated mineralization. *J. Asian Earth Sci.* 88, 149–167.
- Li, J.H., Zhang, Y.Q., Dong, S.W., Johnston, S.T., 2014c. Cretaceous tectonic evolution of South China: a preliminary synthesis. *Earth. Rev.* 134, 98–136.
- Li, B., Jiang, S.Y., Zhang, Q., Zhao, H.X., Zhao, K.D., 2015. Cretaceous crust–mantle interaction and tectonic evolution of Cathaysia Block in South China: evidence from pulsed mafic rocks and related magmatism. *Tectonophysics* 661, 136–155.
- Li, L., Lin, S., Xing, G., Davis, D.W., Jiang, Y., Davis, W., Zhang, Y., 2016a. Ca. 830 Ma back-arc type volcanic rocks in the eastern part of the Jiangnan orogen: implications for the Neoproterozoic tectonic evolution of South China Block. *Precambrian Res.* 275, 209–224.
- Li, B., Jiang, S.Y., Lu, A.H., Zhao, H.X., Yang, T.L., Hou, M.L., 2016b. Zircon U–Pb dating, geochemical and Sr–Nd–Hf isotopic characteristics of the Jintonghumonzonitic rocks in western Fujian Province, South China: implication for Cretaceous crust–mantle interactions and lithospheric extension. *Lithos* 260, 413–428.
- Li, B., Jiang, S.Y., Zhang, Q., Zhao, H.X., Zhao, K.D., 2016c. Geochemistry, geochronology and Sr–Nd–Pb–Hf isotopic compositions of Middle to Late Jurassic syenite–granodiorites–dacrûte in South China: petrogenesis and tectonic implications. *Gondwana Res.* 35, 217–237.
- Li, H., Yonezu, K., Watanabe, K., Tindell, T., 2017a. Fluid origin and migration of the Huangshaping W–Mo polymetallic deposit, South China: geochemistry and $^{40}\text{Ar}/^{39}\text{Ar}$ geochronology of hydrothermal K-feldspars. *Ore Geol. Rev.* 86, 117–129.
- Li, H., Sun, H.S., Wu, J.H., Evans, N.J., Xi, X.S., Peng, N.L., Cao, J.Y., Gabo-Ratio, J.A.S., 2017b. Re–Os and U–Pb geochronology of the Shazigou Mo polymetallic ore field, Inner Mongolia: implications for Permian–triassic mineralization at the northern margin of the North China Craton. *Ore Geol. Rev.* 83, 287–299.
- Li, H., Wu, Q.H., Evans, N.J., Zhou, Z.K., Kong, H., Xi, X.S., Lin, Z.W., 2018a. Geochronology and geochronology of the Banxi Sb deposit: implications for fluid origin and the evolution of Sb mineralization in central-western Hunan, South China. *Gondwana Res.* 55, 112–134.
- Li, H., Palinkaš, L.A., Watanabe, K., Xi, X.S., 2018b. Petrogenesis of Jurassic A-type granites associated with Cu–Mo and W–Sn deposits in the central Nanling region, South China: relation to mantle upwelling and intra-continental extension. *Ore Geol. Rev.* 92, 449–462.
- Li, H., Wu, J.H., Evans, N.J., Jiang, W.C., Zhou, Z.K., 2018c. Zircon geochronology and geochemistry of the Xianghualing A-type granitic rocks: insights into multi-stage Sn–polymetallic mineralization in South China. *Lithos* 312–313, 1–20.
- Li, H., Myint, A.Z., Yonezu, K., Watanabe, K., Algeo, T.J., Wu, J.H., 2018d. Geochemistry and U–Pb geochronology of the Wagone and Hermyingyi A-type granites, southern Myanmar: implications for tectonic setting, magma evolution and Sn–W mineralization. *Ore Geol. Rev.* 95, 575–592.
- Li, H., Li, J.W., Algeo, T.J., Wu, J.H., Cisse, M., 2018e. Zircon indicators of fluid sources and ore genesis in a multi-stage hydrothermal system: the Dongping Au deposit in North China. *Lithos* 314–315, 463–478. <https://doi.org/10.1016/j.lithos.2018.06.025>.
- Liu, C.Z., Liu, Z.C., Wu, F.Y., Chu, Z.Y., 2012. Mesozoic accretion of juvenile sub-continental lithospheric mantle beneath South China and its implications: geochemical and Re–Os isotopic results from Ningyuan mantle xenoliths. *Chem. Geol.* 291, 186–198.
- Ludwig, K.R., 2003. User's Manual for Isoplot 3.00: A Geochronological Toolkit for Microsoft Excel. Berkeley Geochronology Center Special Publication, No. 4 p. 70.
- Machowiak, K., Stawikowski, W., 2012. The Baga-Gazriin Chuluu A-type granites of Central Mongolia compared with other igneous bodies nearby: a geochemical approach. *Geol. Q.* 56, 457–474.
- Mao, J.W., Xie, G.Q., Guo, C.L., Chen, Y.C., 2007. Large-scale tungsten-tin mineralization in the Nanling region, South China: metallogenetic ages and corresponding geodynamic processes. *Acta Petrol. Sin.* 23, 2329–2338 (in Chinese with English abstract).
- Mao, J.W., Cheng, Y.B., Chen, M.H., Pirajno, F., 2013. Major types and time-space distribution of Mesozoic ore deposits in South China and their geodynamic settings. *Miner. Depos.* 48, 267–294.
- Mao, J.R., Li, Z.L., Ye, H.M., 2014. Mesozoic tectono-magmatic activities in South China: retrospect and prospect. *Sci. China – Earth Sci.* 57, 2853–2877.
- Maulana, A., Imai, A., Leeuw, T.V., K, Watanabe, Yonezu, K., Nakano, T., Boyce, A., Page, L., Schersten, A., 2016. Origin and geodynamic setting of Late Cenozoic granitoids in Sulawesi, Indonesia. *J. Asian Earth Sci.* 124, 102–125.
- Pang, C.J., Krapež, B., Li, Z.X., Xu, Y.G., Liu, H.Q., Cao, J., 2014. Stratigraphic evolution of a Late Triassic to Early Jurassic intracontinental basin in southeastern South China: A consequence of flat-slab subduction? *Sediment. Geol.* 302, 44–63.
- Patchett, P.J., Tatsumoto, M., 1980. Lu–Hf total–rock isochron for the eucrite meteorites. *Nature* 288, 571–574.
- Patiño Douce, A.E., et al., 1999. What do experiments tell us about the relative contributions of crust and mantle to the origin of granitic magmas. In: Castro (Ed.),

- Understanding Granite: Integrating New and Classical Techniques. Geological Society Special Publications 168, London, pp. 55–75.
- Pearce, J.A., 1996. Sources and settings of granitic rocks. *Episodes* 19, 120–125.
- Peng, J.T., Zhou, M.F., Hu, R.Z., Shen, N.P., Yuan, S.D., Bi, X.W., Du, A.D., Qu, W.J., 2006. Precise molybdenite Re–Os and mica Ar–Ar dating of the Mesozoic Yaogangxian tungsten deposit, central Nanling district, South China. *Miner. Depos.* 41, 661–669.
- Quan, T.J., Kong, H., Fei, L.D., Wang, G., Li, H., Wu, C.M., 2012a. Petrogenesis of granodiorite porphyry in Baoshan deposit: constraints from geochemistry, zircon U–Pb chronology and Hf isotopes. *Chin. J. Nonferrous Metals* 22, 611–621 (in Chinese with English abstract).
- Quan, T.J., Kong, H., Wang, G., Fei, L.D., Guo, B.Y., Zhao, Z.Q., 2012b. Petrogenesis of the granites in the Huangshaping area: constraints from petrochemistry, zircon U–Pb chronology and Hf isotope. *Geotectonica et Metallogenesis* 36, 597–606 (in Chinese with English abstract).
- Quan, T.J., Wang, G., Zhong, J.L., Fei, L.D., Kong, H., Liu, S.J., Zhao, Z.Q., Guo, B.Y., 2013a. Petrogenesis of granodiorites in Tongshanling deposit of Hunan province: constraints from petrogeochemistry, zircon U–Pb chronology and Hf isotope. *J. Mineral. Petrol. Econ. Geol.* 33, 43–52 (in Chinese with English abstract).
- Quan, T.J., Xi, X.S., Kong, H., Wu, Q.H., Chen, Z.F., 2013b. Yanshanian triple junction tectonic pattern and metallogenesis in southern Hunan, China. *Chin. J. Nonferrous Metals* 23, 2613–2620 (in Chinese with English abstract).
- Rollinson, H., 1993. Using Geochemical Data: Evaluation, Presentation, Interpretation. Longman, Essex p. 325.
- Rutanen, H., Andersson, U.B., Väistönen, M., Johansson, Å., Fröjdö, S., Lahaye, Y., Eklund, O., 2011. 1.8 Ga magmatism in southern Finland: strongly enriched mantle and juvenile crustal sources in a post-collisional setting. *Int. Geol. Rev.* 53, 1622–1683.
- Sarjoughian, F., Kananian, A., Haschke, M., Ahmadian, J., 2016. Transition from I-type to A-type magmatism in the Sanandaj–Sirjan Zone, NW Iran: an extensional intra-continental arc. *Geol. J.* 51, 387–404.
- Shu, L.S., Zhou, X.M., Deng, P., Wang, B., Jiang, S.Y., Yu, J.H., Zhao, X.X., 2009. Mesozoic tectonic evolution of the Southeast China block: new insights from basin analysis. *J. Asian Earth Sci.* 34, 376–391.
- Sun, S.S., McDonough, W.F., 1989. Chemical and isotopic systematics of oceanic basalts: implication for mantle composition and processes. In: Saunders, A.D., Norry, M.J. (Eds.), *Magmatism in the Ocean Basins*. Geological Society Special Publications 42, London, pp. 313–345.
- Sun, H.S., Li, H., Evans, N.J., Yang, H., Wu, P., 2017a. Volcanism, mineralization and metamorphism at the Xiteshan Pb–Zn deposit, NW China: insights from zircon geochronology and geochemistry. *Ore Geol. Rev.* 88, 289–303.
- Sun, H.S., Li, H., Danišk, M., Xia, Q.L., Jiang, C.L., Wu, P., Yang, H., Fan, Q.R., Zhu, D.S., 2017b. U–Pb and Re–Os geochronology and geochemistry of the Donggebi Mo deposit, Eastern Tianshan, NW China: insights into mineralization and tectonic setting. *Ore Geol. Rev.* 86, 584–599.
- Sun, H.S., Li, H., Algeo, T.J., Gabo-Ratio, J.A.S., Yang, H., Wu, J.H., Wu, P., 2018. Geochronology and geochemistry of volcanic rocks from the Tanjianshan Group, NW China: implications for the early Palaeozoic tectonic evolution of the North Qaidam Orogen. *Geol. J.* <https://doi.org/10.1002/gj.3268>, in press.
- Sylvester, P.J., 1998. Post-collisional strongly peraluminous granites. *Lithos* 45, 29–44.
- Taylor, S.R., McLennan, S.M., 1985. *The Continental Crust: Its Composition and Evolution*. Oxford Press, Blackwell, pp. 1–312.
- Wang, D.Z., Shen, W.Z., 2003. Genesis of granitoids and crustal evolution of Southeast China. *Earth Sci. Front.* 10, 209–220 (in Chinese).
- Wang, Y.J., Fan, W.M., Guo, F., Li, X., 2001. Petrological and geochemical characteristics of Mesozoic granodiorite intrusions in Southeast Hunan Province, China. *Acta Petrol. Sin.* 17, 169–175 (in Chinese with English abstract).
- Wang, Y.J., Fan, W.M., Guo, F., Peng, T.P., Li, C.W., 2003. Geochemistry of Mesozoic mafic rocks adjacent to the Chenzhou-Linwu fault, South China: implications for the lithospheric boundary between the Yangtze and Cathaysia blocks. *Int. Geol. Rev.* 45, 263–286.
- Wang, Y.J., Fan, W.M., Peter, A., Cawood, Li S.Z., 2008. Sr–Nd–Pb isotopic constraints on multiple mantle domains for Mesozoic mafic rocks beneath the South China Block. *Lithos* 106, 297–308.
- Wang, F.Y., Ling, M.X., Ding, X., Hu, Y.H., Zhou, J.B., Yang, X.Y., Liang, H.Y., Fan, W.M., Sun, W.D., 2011. Mesozoic large magmatic events and mineralization in SE China: oblique subduction of the Pacific plate. *Int. Geol. Rev.* 53, 704–726.
- Wang, Y.J., Fan, W.M., Zhang, G.W., Zhang, Y.H., 2013. Phanerozoic tectonics of the South China Block: key observations and controversies. *Gondwana Res.* 23, 1273–1305.
- Wang, L., Xu, C., Zhao, Z., Song, W., Kynicky, J., 2015. Petrological and geochemical characteristics of Zhaibei granites in Nanling region, Southeast China: implications for REE mineralization. *Ore Geol. Rev.* 64, 569–582.
- Wei, D.F., Bao, Z.Y., Fu, J.M., 2007. Geochemical characteristics and zircon SHRIMP U–Pb dating of the tongshanling granite in Hunan Province, South China. *Geotectonica et Metallogenesis* 114, 482–489 (in Chinese with English abstract).
- Wei, W., Chen, Y., Faure, M., Martelet, G., Lind, W., Wang, Q., Yan, Q., Hou, Q., 2016. An early extensional event of the South China Block during the Late Mesozoic recorded by the emplacement of the Late Jurassic syntectonic Hengshan Composite Granitic Massif (Hunan, SE China). *Tectonophysics* 672–673, 50–67.
- Whalen, J.B., Currie, K.L., Chappell, B.W., 1987. A-type granites: geochemical characteristics, distribution and petrogenesis. *Contrib. Mineral. Petrol.* 95, 407–419.
- Wheeler, G.E., Varne, R., Foden, J.D., Abbott, M.J., 1987. Geochemistry of Quaternary volcanism in the Sunda-Banda arc, Indonesia, and three-component genesis of island-arc basaltic magmas. *J. Volcanol. Geotherm. Res.* 32, 137–160.
- Witt, W.K., Hagemann, S.G., Villanes, C., 2014. Geochemistry and geology of spatially and temporally associated calc-alkaline (I-type) and K-rich (A-type) magmatism in a Carboniferous continental arc setting, Pataz gold-mining district, northern Peru. *Aust. J. Earth Sci.* 61, 17–42.
- Wu, F.Y., Yang, Y.H., Xie, L.W., Yang, J.H., Xu, P., 2006. Hf isotopic compositions of the standard zircons and baddeleyites used in U–Pb geochronology. *Chem. Geol.* 234, 105–126.
- Wu, F.Y., Li, X.H., Zheng, Y.F., Gao, S., 2007. Lu–Hf isotopic systematics and their applications in petrology. *Acta Petrol. Sinica* 23, 185–220.
- Wu, Q.H., Cao, J.Y., Kong, H., Shao, Y.J., Li, H., Xi, X.S., Deng, X.T., 2016. Petrogenesis and tectonic setting of the early Mesozoic Xitian granitic pluton in the middle Qin-Hang Belt, South China: constraints from zircon U–Pb ages and bulk-rock trace element and Sr–Nd–Pb isotopic compositions. *J. Asian Earth Sci.* 128, 130–148.
- Xie, Y.C., Lu, J.J., Ma, D.S., Zhang, R.Q., Gao, J.F., Yao, Y., 2013. Origin of granodiorite porphyry and mafic microgranular enclave in the Baoshan Pb–Zn polymetallic deposit, southern Hunan Province: zircon U–Pb chronological, geochemical and Sr–Nd–Hf isotopic constrains. *Acta Petrol. Sinica* 29, 4186–4213 (in Chinese with English abstract).
- Xu, X.S., 2008. Several problems worthy to be noticed in the research of granites and volcanic rocks in SE China. *Geol. J. China Univ.* 14, 283–294.
- Xu, W., Xu, X., 2015. Early Paleozoic intracontinental felsic magmatism in the South China Block: petrogenesis and geodynamics. *Lithos* 234–235, 79–92.
- Xu, X., Tang, S., Lin, S., 2016. Paleostress inversion of fault-slip data from the Jurassic to Cretaceous Huangshan Basin and implications for the tectonic evolution of southeastern China. *J. Geodyn.* 98, 31–52.
- Yan, Q.S., Shi, X.F., 2016. Geochronology of the Laoshan granitic complex in eastern China and its tectonic implications. *Geol. J.* 51, 137–148.
- Yang, C., Shen, Z.J., Kuang, W.L., Zhang, W.H., 2012. The geological features and mineralogical mechanism of Tungsten-polymetallic deposits in Tongshanling area, Southwestern Hunan: taking Xianglinpu deposit as an example. *Contrib. Geol. Miner. Resour. Res.* 27, 156–161 (in Chinese with English abstract).
- Yang, J.H., Peng, J.T., Zheng, Y.F., Hu, R.Z., Bi, X.W., Zhao, J.H., Huang, J.C., Zhang, B.L., 2016. Petrogenesis of the Mesozoic Shuikoushan peraluminous I-type granodioritic intrusion in Hunan Province, South China: middle–lower crustal reworking in an extensional tectonic setting. *J. Asian Earth Sci.* 123, 224–242.
- Yao, J., Shu, L., Cawood, P.A., Li, Y., 2016. Delineating and characterizing the boundary of the Cathaysia block and the Jiangnan orogenic belt in South China. *Precambr. Res.* 275, 265–277.
- Yu, J., Xu, X., Zhou, X., 2003. Late Mesozoic crust–mantle interaction and lower crust components in South China: a geochemical study of mafic granulite xenoliths from Cenozoic basalts. *Sci. China Ser. D Earth Sci.* 46, 447–460.
- Yu, X.Q., Wu, G.G., Zhao, X.X., Gao, J.F., Di, Y.J., Zheng, Y., Dai, Y.P., Li, C.L., Qiu, J.T., 2010. The Early Jurassic tectono-magmatic events in southern Jiangxi and northern Guangdong provinces, SE China: constraints from the SHRIMP zircon U–Pb dating. *J. Asian Earth Sci.* 39, 408–422.
- Yuan, H.L., Gao, S., Liu, X.M., Li, H.M., Gunther, D., Wu, F.Y., 2004. Accurate U–Pb age and trace element determinations of zircon by laser ablation-inductively coupled plasma-mass spectrometry. *Geostands Newslett.* 28, 353–370.
- Yuan, S.D., Peng, J.T., Hu, R.Z., Li, H.M., Shen, N.P., Zhang, D.L., 2008. A precise U–Pb age on cassiterite from the Xianghualing tin-polymetallic deposit (Hunan, South China). *Miner. Depos.* 43, 375–382.
- Yuan, Y.B., Yuan, S.D., Chen, C.J., Huo, R., 2014. Zircon U–Pb ages and Hf isotopes of the granitoids in the Huangshaping mining area and their geological significance. *Acta Petrol. Sin.* 30, 64–78 (in Chinese with English abstract).
- Zaraisky, G.P., Aksyuk, A.M., Devyatova, V.N., Udratina, O.V., Chevychelov, V.Y., 2009. The Zr/Hf ratio as a fractionation indicator of rare-metal granites. *Petrology* 17, 25–45.
- Zeng, Y.S., Zhu, Y.F., Liu, J.Q., 2001. Carbonaceous material in S-type Xihuashan granite. *Geochim. J.* 35, 145–154.
- Zhang, J.X., Tong, Q.M., Li, R.Q., 2000. Regional geochemical characteristics across the Chenzhou-Linwu deep seated fault. *Geol. Miner. Resour. South China* 3, 17–24 (in Chinese with English abstract).
- Zhang, Q., Jin, W.J., Li, C.D., Wang, Y.L., 2009. Yanshanian large-scale magmatism and lithosphere thinning in Eastern China: Relation to large igneous province. *Earth Sci. Front.* 16 (2), 21–51 (in Chinese with English abstract).
- Zhang, R.Q., Lu, J.J., Wang, R.C., Yang, P., Zhu, J.C., Yao, Y., Gao, J.F., Li, C., Lei, Z.H., Zhang, W.L., Guo, W.M., 2015. Constraints of in situ zircon and cassiterite U–Pb, molybdenite Re–Os and muscovite ^{40}Ar – ^{39}Ar ages on multiple generations of granitic magmatism and related W–Sn mineralization in the Wangxianling area, Nanling Range, South China. *Ore Geol. Rev.* 65, 1021–1042.
- Zhang, X.S., Xu, X.S., Xia, Y., Liu, L., 2016a. Early Paleozoic intracontinental orogeny and post-orogenic extension in the South China Block: insights from volcanic rocks. *J. Asian Earth Sci.* 141, 24–42. <https://doi.org/10.1016/j.jseas.2016.07.016>.
- Zhang, X.R., Zhao, G.C., Sun, M., Eizenhofer, P.R., Han, Y.G., Hou, W.Z., Liu, D.X., Wang, B., Liu, Q., Xu, B., 2016b. Tectonic evolution from subduction to arc-continent collision of the Junggar ocean: constraints from U–Pb dating and Hf isotopes of detrital zircons from the North Tianshan belt, NW China. *Geol. Soc. Am. Bull.* 128, 644–660.
- Zhao, G.C., 2016. Jiangnan Orogen in South China: developing from divergent double subduction. *Gondwana Res.* 27, 1173–1180.
- Zhao, G.C., Cawood, P.A., 2012. Precambrian geology of China. *Precambr. Res.* 222–223, 13–54.
- Zhao, Z.H., Bao, Z.W., Zhang, B.Y., 1998. Geochemical characteristics of the mesozoic basalts in Hunan Province. *Sci. China (Ser. D)* 28, 7–14.
- Zhao, X.F., Zhou, M.F., Li, J.W., Wu, F.Y., 2008. Association of Neoproterozoic A- and I-type granites in South China: implications for generation of A-type granites in a subduction-related environment. *Chem. Geol.* 257, 1–15.
- Zhao, K.D., Jiang, S.Y., Yang, S.Y., Dai, B.Z., Lu, J.J., 2012. Mineral chemistry, trace elements and Sr–Nd–Hf isotope geochemistry and petrogenesis of Cailing and Furong

- granites and mafic enclaves from the Qitianling batholith in the Shi-Hang zone, South China. *Gondwana Res.* 22, 310–324.
- Zhao, P.L., Yuan, S.D., Mao, J.W., Santosh, M., Li, C., Hou, K.J., 2016. Geochronological and petrogeochemical constraints on the skarn deposits in Tongshanling ore district, southern Hunan Province: Implications for Jurassic Cu and W metallogenic events in South China. *Ore Geol. Rev.* 78, 120–137.
- Zhou, X.M., Li, W.X., 2000. Origin of Late Mesozoic igneous rocks in Southeastern China: implications for lithosphere subduction and underplating of mafic magmas. *Tectonophysics* 326, 269–287.
- Zhou, X.M., Sun, T., Shen, W.Z., Shu, L.S., Niu, Y.L., 2006. Petrogenesis of Mesozoic granitoids and volcanic rocks in South China: a response to tectonic evolution. *Episodes* 29, 26–33.
- Zhu, J.C., Wang, R.C., Zhang, P.H., Xie, C.F., Zhang, W.L., Zhao, K.D., Xie, L., Yang, C., Che, X.D., Yua, P., Wang, L.B., 2009. Zircon U–Pb geochronological framework of Qitianling granite batholith, middle part of Nanling Range, South China. *Sci. China Ser. D Earth Sci.* 52, 1279–1294.
- Zhu, J.C., Wang, R.C., Liu, J.J., Zhang, H., Zhang, W.L., Xie, L., Zhang, R.Q., 2011. Fractionation, evolution, petrogenesis and mineralization of Laiziling Granite Pluton, Southern Hunan Province. *Geol. J. China Univ.* 17, 381–392 (in Chinese with English abstract).